AWARD NUMBER: W81XWH-19-1-0696

TITLE: Understanding the role of gene-environment interactions in the degeneration of human dopaminergic neurons in Parkinson's Disease

PRINCIPAL INVESTIGATOR: Lee Rubin

CONTRACTING ORGANIZATION: President and Fellows of Harvard College
Cambridge, MA 02138

REPORT DATE: January 2023

TYPE OF REPORT: Final

PREPARED FOR: U.S. Army Medical Research and Development Command
Fort Detrick, Maryland 21702-5012

REPORT DOCUMENTATION PAGE

Form Approved
OMB No. 0704-0188

1. REPORT DATE	2. REPORT TYPE	3. DATES COVERED
January 2023	Final	15Sep2019-14Sep2022

4. TITLE AND SUBTITLE
Understanding the role of gene-environment interactions in the degeneration of human dopaminergic neurons in Parkinson's Disease

5a. CONTRACT NUMBER

5b. GRANT NUMBER
W81XWH-19-1-0696

5c. PROGRAM ELEMENT NUMBER

6. AUTHOR(S)
Lee Rubin, PhD

E-Mail: lee_rubin@harvard.edu

5d. PROJECT NUMBER

5e. TASK NUMBER

5f. WORK UNIT NUMBER

7. PERFORMING ORGANIZATION NAME(S) AND ADDRESS(ES)
President and Fellows of Harvard College
1033 Massachusetts Avenue
5th Floor
Cambridge, MA 02139

8. PERFORMING ORGANIZATION REPORT NUMBER

9. SPONSORING / MONITORING AGENCY NAME(S) AND ADDRESS(ES)
U.S. Army Medical Research and Development Command
Fort Detrick, Maryland 21702-5012

10. SPONSOR/MONITOR'S ACRONYM(S)

11. SPONSOR/MONITOR'S REPORT NUMBER(S)

12. DISTRIBUTION / AVAILABILITY STATEMENT
Approved for Public Release; Distribution Unlimited

13. SUPPLEMENTARY NOTES

14. ABSTRACT
Gene environment interactions (GxE) are key to better understanding PD. We are testing pesticides for their effects "in the dish", and in the context of mutations in the synuclein and GBA genes that are also being analyzed in Dr Ritz's epidemiologic cohort. Our experiments will enable us to answer whether key genetic risk factors create sensitivities in patients to particular toxicants and we will ascertain whether gene-toxicant interactions play out specifically at the level of the dopamine neuron. To date, we have generated a unique set of reagents from patients with PD caused by synuclein and GBA mutations and observed differential effects to PD-linked pesticides and toxicants with respect to survival, neurite outgrowth and calcium signaling. From the PEG cohort data and leveraging agricultural pesticide application records (CA-PUR database (discussed below), 1974-2018), we have established long-term exposure profiles for over 200 widely used agricultural pesticides for 1,870 PD patients and population-based controls. Using this data for analysis, we have generated a list of 33 pesticide toxicants that are both significantly associated with PD (FDR<0.01) and have exposure in both α-syn SNPs and GBA variant carriers. This epidemiologic analysis agnostically highlighted, out of pesticides widely used agriculturally in California over the study period, the most significantly associated with PD. In synergy, the lab-based teams (Rubin and Khurana) will in the next phase of research test these epidemiologically derived pesticides in in vitro cell lines in the context of mutations in the synuclein and GBA mechanisms. Validated hits from these screens will then be used in conjunction with SNCA and GBA genetic data to assess GxE interactions with pathway relevant SNPs in the PEG study.

15. SUBJECT TERMS
Parkinson's disease, neurodegeneration, induced pluripotent stem cells, gene-environment interactions (GxE), pesticides, dopaminergic neurons, high throughput screening, familial Parkinson's disease

16. SECURITY CLASSIFICATION OF:			17. LIMITATION OF ABSTRACT	18. NUMBER OF PAGES	19a. NAME OF RESPONSIBLE PERSON
a. REPORT	b. ABSTRACT	c. THIS PAGE			USAMRDC
Unclassified	Unclassified	Unclassified	Unclassified	51	19b. TELEPHONE NUMBER *(include area code)*

TABLE OF CONTENTS

	Page
1. Introduction	4
2. Keywords	4
3. Accomplishments	4
4. Impact	45
5. Changes/Problems	46
6. Products	47
7. Participants & Other Collaborating Organizations	48
8. Special Reporting Requirements	51
9. Appendices	51

1. INTRODUCTION:

Gene environment interactions (GxE) are key to better understanding PD. We are testing epidemiologically identified pesticides for their effects "in the dish" on human dopaminergic neurons and in the context of mutations in the synuclein and GBA genes that are also being analyzed in Dr Ritz's epidemiologic cohort. Our experiments will enable us to answer whether key genetic risk factors create sensitivities in patients to particular toxicants and we will ascertain whether gene-toxin interactions play out specifically at the level of the dopamine neuron. We are constructing exposure profiles for patients harboring common SNPs in α-syn and GBA in the existing epidemiologic data. We are systematically identifying environmental risk factors and pathways that cause selective degeneration of human DA neurons using a screening approach. This project will provide an extensive phenotypic and functional description of the interaction between variably penetrant genetic forms of PD-causing genes and environmental toxicants in well-controlled human DA neurons.

2. KEYWORDS:

Parkinson's disease, neurodegeneration, induced pluripotent stem cells, gene-environment interactions (GxE), pesticides, dopaminergic neurons, high throughput screening, familial Parkinson's disease.

3. ACCOMPLISHMENTS:

What were the major goals of the project?

Specific Aim 1: Determine whether synuclein triplication and GBA mutations increase susceptibility of DA neurons to known environmental toxicants
Major Task 1: Modify cell lines with THtd reporter
Major Task 2: Establish baseline responses to toxicants in the SNCA triplication line and compare exposure phenotypes across other mutations
Major Task 3: Establish exposure profiles for α-syn and GBA SNPs from PEG database
Major Task 4: Test toxicant lists from PEG data in corresponding in vitro cell lines

Specific Aim 2: Systematically identify environmental risk factors and pathways that cause selective degeneration of human DA neurons.
Major Task 5: Assay development to optimize timing of Experiment 1+2 (toxin and custom library screens)
Major Task 6: Perform Screens on DA neurons
Major Task 7: Validated hits from screen used to identify pathway-relevant SNPs for evaluation in the PEG cohort

What was accomplished under these goals?

1) Major wetlab activities undertaken during the reporting period were primarily the acquisition, modification, and characterization of multiple patient iPSC lines used for insertion of the tyrosine hydroxylase::tdtomato (THtd) reporter construct, toxicant sensitivity primary assays, optimization of secondary assays, performance of secondary assays on multiple isogenic pairs, screening assay development, performing screens, screening result follow up, and performing a counter screen to assess selectivity for dopaminergic neurons. Major activities with the PEG epidemiologic cohort included developing pesticide exposure profiles for all pesticides agriculturally used in Central California based on historical agricultural pesticide use reports and occupational and home pesticide use based on self-report, establishing exposure profiles SNCA and GBA variant carriers, and comparing exposure profiles between patients and controls to select toxicants to be used in future corresponding in vitro cell line experiments. Additionally, the PEG epidemiologic study included assessing *SNCA* and *GBA* gene-set gene-environment (GxE) interactions with the specific pesticides we identified as being associated with PD risk in a 'pesticideome' analysis. We conducted pathway analysis of the identified pesticide hits with additional data and literature mining using the comparative toxicogenomics database to identify genetic regions and SNPs in relevant pathways for genetic and GxE analysis with PD (major task 7, subtask 1 and 2). Another substantial accomplishment during the reporting period includes writing of a manuscript that has been posted on BioRxiv (doi: 10.1101/2022.02.06.479305) and has been accepted pending minor revisions to Nature Communications. This manuscript contains data primarily supported by this award and reported in previous progress reports and below.
2) Specific objectives included:
    a. Modify cell lines with THtd reporter (Major Task 1).
    b. Perform validation and quality control of reporter lines produced (Major Task 1).
    c. Establish baseline responses to toxicants in GBA mutant and corrected lines, E46K mutant and corrected lines, synuclein triplication line, and synuclein knockout line (Major Task 2).
    d. Develop pesticide profiles and specific pesticide quantitative measures from GIS models at occupational and residential addresses, home and garden and occupational pesticide use reporting for all risk variant carriers and controls. Analyses comparing these profiles for PD risk have been carried out in the second half of the year. Separate exposure profiles by SNCA and GBA SNPs have been established (Major Task 3).
    e. Assess toxicants from PEG data in E46K mutant/corrected isogenic pair and GBA mutant/corrected isogenic pair (part of Major Task 4).
    f. Assay development for toxicant and custom screens, build custom toxicant library (part of Major task 5)
    g. Perform compound screen and toxicant screen (Major Task 6, subtask 1 and 2)
    h. Perform counter screen on iNGN cortical neurons derived from synuclein triplication line to assess selectivity/specificity of screen hits for dopamine neurons (Major Task 6, subtask 3)
    i. Establish calcium imaging assay for characterization of toxicant responses

j. Assess for evidence of GxE interaction in the PEG study (n=1870), using pesticide profiles for specific chemicals based on quantitative measures from GIS models and using a SNP-set kernel association test to aggregate individual SNP test statistics for all markers in the *SNCA* and *GBA* genes. (Major Task 3 & 7)
k. Assess pesticides associated with PD in PEG (FDR <0.05) for evidence of gene level GxE interaction (Major Task 3 & 7). Major task 7 (next research period) will involve identifying disease pathway-relevant SNPs for evaluation in the PEG cohort.
l. Conduct pathway analysis of pesticide hits, using data and literature mining to identify genetic regions and SNPs in relevant pathway components (Major Task 7, subtask 1)
m. Evaluation of SNPs identified in pathway analysis in PEG cohort for association with PD (Major Task 7, subtask 2)

3) **THtdTomato knock-in line production:** Upon acquiring the GBA mutant and corrected lines from the NINDS repository, we performed a genotyping PCR using published primers. Sequencing of the product to confirm the A to G mutation which results in the N370S mutation. Following the CRISPR-Cas9 mediated knock in of the THtdtomato reporter construct, we recovered multiple clones from both the GBA mutant iPSC line and the GBA corrected iPSC line that passed the necessary PCR quality controls. This includes detecting appropriately sized PCR products with primers designed to flank the 5' and 3' insertion sites, followed by Sanger sequencing of these bands to confirm proper insertion without frameshift mutations or other recombination errors (**Figure 1**). One clone per genotype was then sent to WiCell for karyotyping. Both resultant cell lines have normal karyotypes. These cell lines were then differentiated according to our standard dopamine neuron protocol confirming proper expression of the reporter following exposure to patterning factors as described (Ahfeldt et al 2020, PMID 31902706, **Figure 2**). The SNCA-triplication line was validated and subjected to the same quality control workflow as described above for the generation of the GBA lines. We added an additional quality control step to assess for non-homologous end joining errors by Sanger sequencing of the CRISPR site at the unmodified TH locus. This additional step was added because we discovered occasional NHEJ errors occur at the non-modified locus in other cell lines. Three clones passed all aspects of quality control but only one clone (clone #48, **Figure 1**) was sent for karyotyping to reduce costs. This line has a normal karyotype, demonstrates bright, appropriate expression of the THtdtomato reporter and was therefore used for subsequent experiments and for the screens in major task 6 and 7 (**Figure 2**).

There were not any dramatic morphological or differentiation phenotypes observed when comparing the GBA mutant and corrected lines. THtdtomato(+) neurons from both lines are similar in morphology to one another and their appearance is consistent with other published knock-in lines generated with this reporter (Ahfeldt et al 2020). Multiple clones from both lines generated typical percentages of dopamine neurons (50-70%) as demonstrated by FACS analysis and imaging following our published floor plate patterning differentiation protocol. Production of the SNCA knockdown and knockout lines was substantially more time consuming and challenging than the other THtdtomato lines generated for this project. Previous experience with the recombination plasmid template and guide RNA plasmids used for the reporter knock in resulted in about 40-50% of clones with a NHEJ error on the unmodified allele of tyrosine hydroxylase, typically with a length of 7-14 bases. The potential knock-in clones recovered from the synuclein knockdown and knockout lines showed substantially higher frequency of NHEJ errors (approximately 70-90% of clones) and the errors were larger than those previously encountered in other lines (**Figure 3**). This may be a function of the parental line itself or a function of a role for alpha-synuclein protein in DNA repair processes/NHEJ (Schaser et al Sci Reports 2019). Failure to recover viable clones that passed all the typical QC steps due to this increased frequency of NHEJ errors required an iterative process that has increased the time needed to recover clones and required picking and analyzing 4-5x the normal number of colonies for propagation and analysis. Two THtdtomato clones from the SNCA knockout line passed all QC steps and was used for primary and secondary assays as a comparison to the SNCA triplication line. Due to budget and time constraints, attempts to recover a THtdtomato knock-in clone for the 2-copy isogenic line have been suspended. Limited analysis was performed on mixed cultures of the unmodified parental 2-copy clone using antibody staining for tyrosine hydroxylase and other neuronal markers to provide the necessary comparison data on toxicant sensitivity.

Survival Assays with Established Pesticides: Following generation and validation of the SNCA-triplication line described above, screening assay development and toxicant response profiles were initiated. FACS purified THtdtomato dopaminergic neurons were compared to mixed cultures containing other non-THtdtomato expressing cells. The primary readouts of the assay were survival and neurite length. Comparison of the sorted and mixed cultures indicated that sensitivity (to both cell death and neurite loss) to a subset of toxicants was either very similar in both assay conditions, or the sorted cells showed increased sensitivity compared to mixed (**Table 1**). This result indicated that using FACS sorted THtdtomato dopaminergic neurons for the compound and toxicant screens provides the most sensitive and easily quantified readout of cell death and neurite loss. The unprecedented need to suspend wet lab work for an extended period of time during the first few months of the COVID-19 pandemic afforded us the opportunity to assess whether cryopreserved dopaminergic neurons could be used for the survival and neurite growth assays. A limited assessment of these cryopreserved neurons suggested that they are not optimal for the assays due to variable survival after thawing. However, batches that showed good survival after thawing did demonstrate comparable sensitivity to toxicants with respect to neurite length when compared to freshly assayed cells from the same cell line (data not shown). After establishing baseline responses to a subset of toxicants with freshly differentiated dopaminergic neurons from the SNCA-triplication line, we expanded the analysis to the GBA mutant and GBA corrected lines, again focusing on sorted THtdtomato dopaminergic neurons.

These experiments suggest that the SNCA-triplication line may be more sensitive to paraquat and rotenone while having similar sensitivity to permethrin (**Figure 4**). Prior to the generation of the SNCA-triplication reporter line and the GBA reporter lines, we began to characterize the response of the E46K synuclein mutant line to a subset of the toxicants described in Table 3 of the Project Narrative. For all toxicant experiments, live images were acquired 11 days after treating sorted dopaminergic neurons with toxicants and image analysis revealed different sensitivities to toxicants, with ziram showing the most potent toxicity and cyanazine showing the least toxicity (**Figure 4**). The toxicant responses for each of these lines has provided insight into variation in sensitivity to the initial set of toxicants as a function of cell line and genotype. The aggregated and normalized results provided a few important insights: 1) the sensitivity to toxicants varied greatly based on the toxicant used, with ziram being the most potent toxicant in all cells lines tested and cyanazine being the least potent in all cell lines tested; 2) Differences in sensitivity to toxicants were more pronounced between cell lines than between isogenic pairs with the exception of paraquat where E46K mutant synuclein appeared to result in higher sensitivity than the corrected control; 3) Replicates with the A07-E46K isogenic pair (mutant and corrected) showed less sensitivity to ziram, compared to the other lines used in the analysis. The finding that mutations in synuclein or GBA do not confer increased sensitivity to most toxicants tested in this small subset is not surprising given that this set of toxicants was derived from a cohort of PD patients that did not take into account mutations or SNPs in SNCA or GBA. This limited set of toxicants did provide useful assay parameters for the design of the toxicant screen and has helped with selection of the upper and lower limits of dosing used for that screen.

Screen Assay Development and Performance of Pesticide Survival Screen: Assay planning and development for the toxicant screen and compound screen were completed. The "pesticide wide association study" or "PWAS" pesticide list (see Ritz lab section and our attached manuscript for a more detailed description of the PWAS) provided by the Ritz lab was classified by solubility in DMSO, water, or ethanol in preparation for screening library construction. Acquisition, resuspension, and aliquoting of these toxicants was completed. Of the 64 toxicants, three have very high dermal toxicity in humans and mammals, making their use problematic from an occupational health and safety standpoint. These were omitted from testing. Eighteen were soluble in DMSO, twenty-three were soluble in water and seventeen were soluble in ethanol. Different template plates were generated for each solvent. Four concentrations for each toxicant were assayed in duplicate (water soluble toxicants) or triplicate (DMSO and ethanol soluble toxicants) in the toxicant screen. The concentrations were chosen based on solubility, previously published toxicant/pesticide-based screens and experience with other toxicants in Aim 1. Data from this custom toxicant library simultaneously addressed objectives stated in Major Task 4, subtask 1 for the SNCA triplication line, and Major Task 6, subtask 1. Performing the assay in this manner is more cost effective because the SNP-associated PEG/PWAS toxicants are contained in the custom screening library.

Results from the toxicant screen indicated a successful dynamic range between negative controls (DMSO, water, DMSO+Ethanol) and positive controls (rotenone, ziram). The Z prime score for DMSO as the negative control and rotenone positive control was 0.549. The following toxicants produced cell death >4 standard deviations below the mean at the 30uM screening concentration: propargite, copper sulfate (basic and pentahydrate), folpet, dicofol, naled, endothall, trifluralin, endosulfan, and diquat dibromide (**Figure 5A**)

A few additional toxicants had cell death between 2-4 standard deviations below the mean or had large well to well variability in the screen. Secondary assays and biochemistry were performed on the subset of the toxicants that clearly resulted in extensive cell death (>4 standard deviations). Four-concentration dose response curves designed into the screening library indicated that propargite is the most toxic, followed by diquat dibromide, folpet, and naled—all of which are also toxic at 6uM (**Figure 5C**). Our finding that propargite causes dopaminergic neuron cell death provides an independent validation of other studies which also identified this toxicant in screening assays (Zhou, T. Nat Communications 2018). Multiple toxicants identified in our custom screen of the PEG/PWAS toxicants remain actively registered with the EPA and are used in agriculture. Evidence that they directly cause death of dopaminergic neurons *in vitro* could have implications for usage and policy decisions. Secondary assays performed by collaborators in the Khurana lab provides additional mechanistic detail for a subset of these toxicants (see below).

Orthogonal validation of toxic pesticides: Imaging-based measurements of cell health, including neurite length, cell area, and pixel intensity of THtdT reporter were measured independent of cell count to confirm toxicity (**Figure 6A, D, E**). The toxicity data determined by cell counts presented in Figure 5 relies upon fluorescence from the THtdTomato knock in construct. A pesticide that dramatically reduced expression of the TH gene or greatly exacerbated degradation of the THtdTomato reporter without causing cell death could produce a false positive in this experiment. We thus performed an orthogonal viability assay using CellTitreGlo (Promega) according to the same experimental conditions as in Figure 5 on a subset of pesticides identified as toxic in the initial screen. Viability decreased as expected with concentrations at or below the original screening concentration (**Figure 7**, n=1).

Parallel samples of sorted THtdtomato+ neurons from SNCA triplication and SNCA knockout reporter lines were exposed to a subset of toxicants identified in the original screen. Compounds causing cell death in the triplication line also caused cell death in the knockout line at concentrations at or below the original screening concentration of 30µM (**Figure 8**). Experiments demonstrated a trend towards increased sensitivity of the SNCA knockout neurons to folpet, naled, propargite, and trifluralin as shown by comparisons of cell counts normalized to the DMSO control for each cell line (**Figure 9**). Sensitivity to dicofol, endosulfan, endothall and ziram was not markedly altered by SNCA knockout. Testing of PEG/PWAS toxicants in the E46K mutant line indicated sensitivity to many of the same toxicants that caused cell death in the SNCA triplication line, with a few notable differences. Copper compounds caused less death in the E46K line than in the SNCA triplication line and oryzalin produced more cell death in the E46K neurons than in the SNCA triplication dopaminergic neurons (**Figure 10**). Comparisons with the isogenic corrected control suggested that this sensitivity to oryzalin was a function of line-to-line sensitivity differences rather than a function of the E46K mutation itself because the E46K-corrected line was as sensitive or more sensitive to oryzalin than the mutant line.

Bioactive Compound Screen: As described in the project narrative, we also undertook a more traditional compound screen using a subset of compounds from a commercially available bioactive compound library (SelleckChem Bioactive library). The number of screened compounds was 776. This was a subset of the full library (>3,000 compounds) and was chosen to overrepresent compounds with targets involved in neuronal signaling pathways and inflammation. In the live imaging screen, surviving cells and neurite length were measured using a Molecular Devices IXM high content microscope. Image analysis using Columbus (Perkin Elmer) software was designed to select cells based on area, roundness, and THtdtomato signal intensity. Exported data was then processed using GeneData Screener software to perform Robust Z score normalization of the data.

Berzosertib, an ATR inhibitor identified in a previous toxicity screen in the Rubin lab (unpublished) on E46K-synuclein mutant dopamine neurons was used as the positive control. The compounds resulting in cell death >3 standard deviations greater than the DMSO control wells and their corresponding annotations supplied by the commercial vendor are provided in **Table 2**. To provide an overview of which pathways are over-represented among the hit compounds, the percentage of various pathway annotations in the screened compounds were calculated and compared to the frequency of pathway annotations among the hit compounds. Pathways involving apoptosis, cytoskeletal signaling, microbiology, NFkB, transmembrane transporters and ubiquitin were overrepresented in the list of hit compounds compared to the input compound library. Multiple compounds affecting dopamine receptor activity are also among the toxic compounds. A subset of these compounds were validated by dose response curves (see below).

The SelleckChem compound screen was repeated on NGN2-induced cortical neurons generated from a modified version of the SNCA triplication line allowing for robust production of cortical neurons. This counterscreen was performed with the goal of providing information about the specificity and relative potency of compounds identified in the dopamine neuron screen. This screen used the exact same library of 776 compounds that was screened in THtdtomato+ dopaminergic neurons. As in that screen, compounds were tested in triplicate plate format at a concentration of 3μM. The readout for this screen required immunostaining for a neuronal marker and more detailed image analysis to establish measures of toxicity. MAP2 staining was used as a measure of neurite length and as a way to count surviving cells (MAP2 staining in the perinuclear cytoplasm of a Hoechst positive nucleus was counted as a surviving cell, while Hoechst positivity alone were regarded as dead or dying nuclei). Berzosertib, a compound with previously established toxicity in our preliminary data on dopaminergic neurons from a different iPSC line was used as the positive control. The RZ prime value for the cell count criteria was 0.053. Measurement of neurite length provided a more sensitive measurement of toxicity in this assay and provided greater separation between positive and negative controls with an increased dynamic range of the assay. The RZ prime value for neurite length measurements was 0.419—which is more comparable to the quality of the dopamine neuron screen (RZ prime = 0.314). Based on cell counts, there were 43 compounds identified in the screen of iNGN2 cortical neurons derived from the SNCA triplication iPSC line that showed cell death 2 standard deviations or more greater than DMSO control at the screening concentration of 3μM (below green box in **Figure 12**). Twenty-five of these were also identified as hits in the previously reported dopamine neuron screen. Eighteen were unique to the cortical neuron screen. For comparison, the dopamine neuron screen identified 73 compounds as hits at least 2 standard deviations greater than DMSO control. Forty-eight are unique to the dopamine neurons and not shared with cortical neurons (see **Table 3** and **Table 4**). Pathways implicated regulation of NFkB and modulation of neurotransmitter signaling as important for dopamine and cortical neuron survival. The differential sensitivity will be used to guide further follow up, such that compounds of interest with more selectivity for dopamine neurons will be prioritized over those with shared toxicity with cortical neurons. Nine-point dose curves have been completed for hit validation on a subset of these compounds (**Figure 13**). Fourteen compounds were chosen for this extended dose curve validation. Ten validated at or below the screening concentration. Two compounds showed toxicity, but at a higher concentration than the screening concentration (JNK-IN-8 and benzydamine).

Two compounds did not validate (beclomethasone and ropinirole). Possibilities include variability in the maturation or differentiation of dopamine neurons used in the validation experiment or reduction of potency while compounds were in storage. Notably, QNZ (EVP4593) had a very potent dose response with moderate toxicity at 3nM doses. This compound is the most potent of the NFkB pathway-targeting compounds that have been screened.

In prior reports, the Khurana lab described optimization of assays in iPSC-derived dopaminergic neurons. This optimization has continued, as noted below, particularly to cope with the challenges of the long-term dopaminergic neuron cultures required to generate electro physiologically active neurons that are essential for measuring calcium fluxes. Beyond this optimization, in this last 6 months, important progress has been made using these optimized assays to study the effects of specific pesticide/toxicants identified by the Ritz group and screened by the Rubin group.

Significant results from the Khurana lab are related to Task 2 (Subtasks 2 and 3, 4) and Task 4 (subtask 2). We have focused our efforts on following up the standardization of the most robust assays described in the neuronal functionality assay toolbox **(Figure 14)**. As reported previously, we used the mitochondrial subunits assay to evaluate the effect of selected toxicants on mitochondria stability. This western blot based mitochondrial function assay **(Figure 15)** allowed the assessment of the relative amounts of respiratory chain complexes, Complex I (assessed by NDUFB8), Complex II (assessed by SDHA and SDHB), Complex III (assessed by UQCRC2), Complex IV (assessed by COX II), Complex V (assessed by ATP5A), TOMM20 and actin. This assay was optimized on the SNCA triplication (S3W) cell line using Trifluralin, Propargite and Ziram as tested toxicants. **Figure 15A** describes the work flow to obtain the THtdtomato SNCA triplication differentiated neurons and time of exposure to Trifluralin in 8 wells of 24 well plate format. Embryoid bodies were dissociated to obtain a mixed (unsorted) culture of SNCA triplication neurons as described in **Figure 15B (i)** and **(ii)**. Two million cells per well were seeded and exposed to Trifluralin at different concentrations for 6 and 24 hours. A significant change in protein expression in the mitochondrial subunit assay **(Figure 15C) (i)** is demonstrated by the quantification of complex I **(Figure 15C) (ii)** and complex IV **(iii)**, when differentiated SNCA triplication neurons are exposed to 30μM Trifluralin. All the samples were normalized to actin.

We gained substantial experience on the standardization of the Agilent Seahorse XFCell Mito stress assay. With this assay, we can measure multiple physiologic parameters of differentiated neurons, providing information about mitochondrial function and health. **Figure 16A** describes the work flow to obtain the THtdtomato SNCA triplication differentiated neurons, the time of exposure to Trifluralin and the time for the neuronal respiration / mito-stress assay. This assay provided information about the oxygen content in extracellular media; the oxygen consumption rate (OCR); the extracellular proton concentration (pH); and the extracellular acidification rate (ECAR). We used this assay to characterize the effect of different concentrations of Trifluralin [90μM, 60μM, 30μM and 10μM] on mixed culture of differentiated THtdtomato neurons of the cell lines depicted in **Figure 16B.** Data from the following lines are shown: SNCA-triplication (S3W) **(i)** and its isogenic knockout, SNCA-null (E9) **(ii);** E46K-par1 (also referred to as A07-mutant) **(iii)** and its isogenic corrected clone, E46K-Corr (also referred to as A07-corrected) **(iv);** and GBA-mutant **(v)** and its isogenic corrected clone GBA-corrected (iv).

Notice that trifluralin has a higher effect on the reduction of the spare respiratory capacity on SNCA-null (E9), 99% when exposed to 30μM trifluralin compared to DMSO. Meanwhile, SNCA-triplication (S3W) has 83% reduction when evaluated at the same concentration. Regarding the effect of trifluralin at 60μM, the spare respiratory capacity of E46K-par1 (A07-mut) is reduced 64% and 49 % in the case of E46K-Corr (A07-corr). In the case of GBA mutant and GBA corrected neurons, trifluralin at 60μM reduces the spare respiratory capacity 47% for GBA-mut and 78% in GBA-corr THtdT differentiated neurons compared to DMSO control.

This is representative of a single biological replicate using 6 technical replicates for each cell line. Therefore, confirming this difference will require additional biological replicates to assess whether the trifluralin mediated effect is reproducible.

Substantial progress in the Khurana lab was made in the implementation of reporter assays using genetically encoded indicators (GEI). We chose to move forward with GEI rather than chemical indicators like Fluo-4 and Fura-2 due to the flexibility of GEI for long term and sequential acquisition of calcium imaging data. The evaluation of intracellular calcium in the ER of THtdT differentiated neurons, is based on the use of GECI Calcium-Measuring Organelle-Entrapped Protein Indicators (CEPIA), G-CEPIA1er reported by Suzuki et al. (DOI: 10.1038/ncomms5153), using the lentiviral vector pCMV G-CEPIA1er (Addgene plasmid 58215). To study calcium dynamics and neuronal activity, we used the GECI lenti vector pHAGE-RSV-GCaMP6s (Addgene plasmid 80146) provided by collaborators at the Wainger laboratory (Aaron Held and Brian Wainger) at Massachusetts General Hospital and syn-GCaMP6s from the Woolf laboratory (Lee Barrett and Clifford Woolf) at Boston Children's Hospital. **Figure 17** shows the work flow to obtain the THtdtomato SNCA triplication differentiated neuron, the time for GECI transduction, exposure to toxicants, and time for measurement of calcium dynamics using calcium imaging acquisition protocols. Using GCaMP6 under control of the RSV promoter and the synapsin (syn) promoter allows for analysis of different subpopulations within the culture. We found the synapsin promotor to be best suited for our analysis. The effects of toxicants on differentiated neurons expressing the endoplasmic reticulum (G-CEPIA1er) calcium indicator at DIV 65 was evaluated. **Figure 18** shows the effect of 6 hours exposure to Trifluralin at 60µM **(A)**, Ziram at 1µM **(B)** and Copper Sulfate at 60µM **(C)**. Over the assay timeline, these compounds lead to the formation of intracellular aggregates at the concentrations tested. However, no aggregates are formed at lower concentrations and longer exposure times to the toxicants. Therefore, further characterization and quantification of this effect on differentiated THtdtomato neurons will require a deeper evaluation of optimal conditions to define why these toxicants induce the formation of aggregates in those neurons.

In the final reporting period, significant results in the Khurana lab focused on the use of the calcium image imaging analysis pipeline for the analysis of data obtained from the evaluation of selected toxicants (Trifluralin, Copper Sulfate and Ziram) in E46K-par1 THtdtomato (mutant SNCA) differentiated neurons. For this part of the project, we focused our effort on evaluating the effect of those toxicants on calcium dynamics in this cell line, because neurons obtained from this cell line were robust and performed very well in the syn-GCaMP6 based calcium imaging assay.
A substantial advance in the Khurana lab during the grant period is represented by the increase functionality of the Calcium Signaling Analyzer (CaSiAn) toolbox (Moien et. al. 2018, doi: 10.1093/bioinformatics/bty281.) image analysis pipeline. This automated calcium imaging analysis pipeline combines the versatility of the CaSiAn software tool, with automatic preprocessing, cellular segmentation, fluorescent traces generation, and spike train inference for a given set of time-lapse calcium images. A summary of the work flow of this pipeline is represented in **Figure 19**.
This highlights the main stages in the image analysis process; starting with the acquisition of time lapse images of selected neurons expressing the GCaMP6 GECI and TH-tdtomato reporters in specific regions of interest (ROIs) of selected wells, in 96 well plates, followed by cell segmentation and classification. The use of images acquired in the Texas Red (TH-tdtomato positive cells) and the FITC (GCaMP6) fluorescence channels, is followed by overlapping those segmented images to generate a mask, resulting in the ability to discriminate the spontaneously firing differentiated neurons, which are TH-tdtomato positive from the TH-tdtomato negative neurons.

Following this step, a unique cell identifier (numbering) is assigned to each segmented active cell in selected regions of interest (ROIs). Fluorescent traces and their spike trains (probability of action potentials) are generated for each neuron. Following these automated steps, we use the automatic functionality of CaSiAn tool to quantify various features (spike amplitude, spike width, inter-spike interval or frequency of calcium transient, and calcium releasing and removing rates) of the calcium transient fluorescent traces during the acquisition time. These features are correlated to different aspects of calcium dynamics in the cell and, allow us to describe and compare these parameters between cell lines and treatment conditions. Statistical analysis is the final step in the work flow for the pipeline.

Results from the evaluation of Trifluralin at 2.5µM in our syn-GCaMP6 based calcium imaging assay on E46K-par1 (A07-mut) THtdtomato differentiated neurons, are shown in **Figure 20A**, sample firing traces (calcium transient) and spike trains for DMSO 0.2% **(i)** and trifluralin at 2.5µM **(ii)** after 3hr exposure, as well as pie charts for those two conditions, showing the percentage distribution of active neurons, according to Inter-Spike Interval (ISI) **(iii)**. Cells treated with trifluralin at 2.5µM show 7% increase in hyperactivity (firing at 0-10 sec ISI) and 23 % (firing at 10-20 sec ISI) than those exposed to 0.2% DMSO. A more detailed representation of the distribution of ISI for the two conditions is shown in figure **Figure 20B** and the statistical analysis and significance (t-test) for the Calcium transient signal features, is described in **Figure 20C**, denoting significant differences between the Trifluralin treated and DMSO treated differentiated neurons in all the Calcium transient signal features ($p<0.0001$).

When A07-mut (E46K-synuclein mutant) neurons are exposed to 2.5µM Trifluralin but for 24 hours **Figure 21A**, the hyperactivity represented by the change on ISI at 0-10 sec increases 27% compare to 0.2 % DMSO and 10-20 sec ISI only 2% **(iii)**, indicating that A07-mut neurons become more hyperactive after 24 hr exposure to Trifluralin. Only the Calcium transient signal feature of releasing rate was not statistically significant when compared to DMSO, while the others remain significant with $p<0.0001$. In the case of addressing differences between TH^+ tdtomato ("Dopa") and THtdtomato negative ("Normal") differentiated neurons, after 3hr exposure to 2.5µM Trifluralin, compared to 0.2 % DMSO (**Figure 22A)** only the ISI **(ii)** and the time to peak **(vii)** signal features show significant differences. Nevertheless, after 24hr exposure to those conditions, **Figure 22B** only the ISI **(ii)**, spike width **(vi)** and time to peak **(vii)** signal features show significant differences. At the concentrations tested, no striking differences were seen between TH^+ tdtomato (Dopa) and TH tdtomato negative (Normal) differentiated neurons. If differences exist in this *in vitro* system, longer sublethal toxicant exposures may be necessary to observe differences.

Results from the evaluation of $CuSO_4$ at 2.5µM in our syn-GCaMP6 based calcium imaging assay on E46K-par1 (A07-mut) THtdtomato differentiated neurons, are shown in **Figure 23A**, sample firing traces (calcium transient) and spike trains for DMSO 0.2% **(i)** and $CuSO_4$ at 2.5µM **(ii)** after 24hr exposure, as well as pie charts for those two conditions, showing the percentage distribution of active neurons, according to ISI **(iii)**. Cells treated with $CuSO_4$ at 2.5µM show 12% decrease in hyperactivity (firing at 0-10 sec ISI) and 10 % increase (firing at 10-20 sec ISI) compared to control (0.2% DMSO). A more detailed representation of the distribution of ISI for the two conditions is described in figure **Figure 23B** and the statistical analysis and significance (t-test) for the Calcium transient signal features is described in **Figure 23C**, showing significant differences between the ISI **(ii)**, spike width **(vi)** and time to peak **(vii)** signal features for $CuSO_4$ treated and DMSO treated differentiated neurons ($p<0.0001$).

When A07-mut neurons are exposed for 24 hours at a $CuSO_4$ concentration of 15µM (**Figure 24A)**, the hyperactivity represented by the change on ISI at 0-10 sec decreases by 3 % compare to 0.2 % DMSO, and the 10-20 sec ISI also decrease 3% **(iii)**, suggesting that A07-mut neurons become less hyperactive than control after 15µM exposure to $CuSO_4$ for 24hr. The same Calcium transient signal features of ISI **(ii)**, spike width **(vi)** and time to peak **(vii)** continued being significant with $p<0.0001$. In the case of addressing differences between TH^+ tdtomato (Dopa) and none TH tdtomato (Normal) differentiated neurons, after 24hr exposure to 2.5µM $CuSO_4$, compared to 0.2 % DMSO **Figure 25A**, only the Amplitude **(i)** and the Releasing Rate **(iv)** signal features show significant differences ($p<0.001$). However, none of the Calcium signal features show significant differences after 24hr exposure to $CuSO_4$ at 15µM, **Figure 25B**. Further studies using a copper ionophore to facilitate copper uptake into neurons may facilitate addressing the effectiveness of this toxicant in A07-mut differentiated neurons.

Results from the evaluation of Ziram at 50nM in our synapsin-GCaMP6 based calcium imaging assay on E46K-par1 (A07-mutant) THtdtomato differentiated neurons, are shown in **Figure 26A**. Sample firing traces (calcium transient) and spike trains for DMSO 0.2% **(i)** and Ziram at 50nM **(ii)** after 3hr exposure, as well as pie charts for those two conditions, showing the percentage distribution of active neurons, according to ISI **(iii)** are shown. Cells treated with Ziram at 50nM show 2% decrease in hyperactivity (firing at 0-10 sec ISI) and 1% increase (firing at 10-20 sec ISI) than those exposed to 0.2% DMSO. A more detailed representation of the distribution of ISI for the two conditions is described in figure **Figure 26B** and the statistical analysis and significance (t-test) for the Calcium transient signal features is described in **Figure 26C**. Of note, no significant differences were seen for any of the signal features for Ziram treated compared with control for this set of experiments at the shorter time interval of 3 hours.

When A07-mut neurons are exposed to 50nM Ziram but for 24 hours **Figure 27A**, the hyperactivity represented by the change on ISI at 0-10 sec decrease by 4 % compare to 0.2 % DMSO and the 10-20 sec ISI increase 3% **(iii)**, meaning that A07-mut neurons become less hyperactive than control after 50nM exposure to Ziram for 24hr. Only the Amplitude **(i)** Calcium transient signal feature become significant with $p<0.001$. In the case of addressing differences between TH^+ tdtomato (Dopa) and none TH tdtomato (Normal) differentiated neurons, after 3hr exposure to 50nM Ziram, compared to 0.2 % DMSO, **Figure 28A** none of the signal features show significant differences. Longer duration of exposure to Ziram does have effects. A dose of 50nM Ziram for 24hr results in significant differences for the Amplitude **(i)**, the Releasing Rate **(iv)** and the Spike-area Calcium signal features ($p<0.001$, **Figure 28B)**. Further studies using Ziram at higher concentration may provide more information on the effect of this toxicant in A07-mut differentiated neurons.

Results from the Ritz lab related to Specific Aim 1 Major Task 3 and Specific Aim 2 Major Task 7 helped us to establish pesticide exposure profiles and quantitative exposure measures, and generate a list of 33 pesticide toxicants that are both formally statistically significantly associated with PD (FDR<0.01) and for which we observed exposure in carriers and non-carriers of *SNCA* SNPs and *GBA* variants. This list of 33 pesticides has been used to test for PD-related toxic mechanism in-vitro cell lines. This set of pesticides also provided the foundation for GxE testing with *SNCA* SNPs and *GBA* variants (see below).

All of our analyses use the Parkinson's Environment and Genes (PEG) study from three agricultural counties in Central California. PEG is a population-based case-control study comprised of two, independent study waves, recruited some ten years apart (wave 1: 2001-2007 & wave 2: 2010-2016; n=849 PD patients, n=1021 population-based controls). We generated pesticide exposure profiles using a GIS-based model, which allows us to estimate ambient exposure to specific pesticides based on long-term residential and occupational proximity to agricultural pesticide applications. We used state-mandated pesticide use reports (CA-PUR database) and GRAPES, a GIS model we developed for ambient pesticide exposures that uses a sophisticated computer algorithm to combine California state mandated commercial pesticide use reports, land use, and participant address histories for exposure assessment. We generated long-term exposure profiles to all pesticides applied in the study area (1974-interview/PD dx (with 10-year lag), nearly 700 pesticides applied in study area). We identified 33 pesticides associated with PD in both the wave 1 discovery and wave 2 validation cohort at a meta-FDR<0.01, a total of 53 pesticides were associated with PD at a meta-FDR<0.05. More detail on this analysis has been provided in our paper (doi: 10.1101/2022.02.06.479305; PDF of manuscript in revision with Nature Communications added as addendum to report).

As a next step, we assessed these PD-associated pesticides in conjunction with *SNCA* and *GBA* genetic data to explore possible GxE interactions. We have previously done GWAS genotyping (with 100k PD markers added for good coverage of PD genes) and exome sequencing (PD patients only) for both the *SNCA* and *GBA* genes. The PEG study has data on variations in 1,061 *SNCA* markers and 321 *GBA* markers (including a 100k bp buffer around the gene). The majority of markers in both the *SNCA* and *GBA* genes have a low or rare minor allele frequency (MAF), which is shown in **Figure 29**. Both rare and common variants are likely important contributors to PD etiology. We therefore assessed these genes as a whole using a SNP-set kernel association test (SKAT). SKAT is a SNP-set level test for association between a set of rare and/or common variants and dichotomous or quantitative phenotypes. SKAT aggregates individual score test statistics of SNPs in a SNP-set and computes SNP-set level p-values, e.g. a gene or a region level p-value, while adjusting for covariates, such as principal components to account for population stratification.

We first tested whether the *SNCA* and *GBA* SNP-sets were associated with PD - as expected - based on large idiopathic PD genetic studies. Our results indicated genetic risk due to variants in these genes in PEG participants, with mainly common variants in *SNCA* but rarer variants in *GBA* found to be associated with PD. This was expected, as meta-GWAS associated GBA variants have low allele frequencies (MAF<0.01), while common *SNCA* variants have previously been identified as risk variants associated with PD. Our findings are detailed below:

			Employing weights allows for assumptions about rare variants			
			No variant weighting (linear) [a]	**Upweighted Rare Variant** (weights.beta =c(1,25))[b]	**Madsen and Browning weights – Common variants** (weights.beta= c(0.5,0.5))[c]	**Combined common and rare**[d]
	Sample Size	**Number of Variants**	**p-value**	**p-value**	**p-value**	**p-value**
SNCA	1501	1061	4.03E-05	0.22	1.54E-05	2.60E-04
GBA	1501	321	0.25	3.89E-03	0.17	0.12

a flat-weight (no weight), no variant weighting
b The weight is designed to incorporate an assumption that rare variants are more likely to be causal variants with larger effect sizes. For common variants, this weighting scheme does not work because it assigns almost zero weight to common variants (e.g., w = 0.0004 for a MAF of 0.30 but w = 7.28 for a MAF of 0.05).
c To incorporate more effects from common variants, the weight slowly decreases with increasing MAF. For example, for MAF = 0.05, $w = 1.46$, for MAF = 0.10, $w = 1.06$, for MAF = 0.30, $w = 0.69$, and for MAF = 0.5, w = 0.64.
d To test for both common and rare variants together, SKAT-CommonRare function uses a weighting scheme in which common and rare variants contribute to the test equally.

After generating the *SNCA* and *GBA* SNP-set summary results and confirming their contributions to PD risk, we next assessed whether there was evidence for GxE interactions. We selected a case-only design, as we have exome sequencing data only available for the patients and also to increase statistical power. In a case-only design, for genetic factors are not interacting with pesticide exposure to influence PD risk, we expect exposure to be similarly distributed across all risk genotypes among PD patients. Thus, to screen for interaction, we first tested whether the SNP-sets were associated with differences in exposure among the PD patients (n=728), controlling for genetic ancestry, sex, and age. We tested all pesticides we previously found to be associated with PD risk and employed two weighting schemes for handling rare and common genetic variants (see footnotes b and c in table above). The results have been visualized in **Figure 30**, which displays the SNP-set p-values between each exposure and the *SNCA* or *GBA* SNP-sets. We found evidence of interaction with two related pesticides and the *SNCA* SNP-set, i.e. with both Dicamba (p=0.001) and Dicamba, other related salt (p=0.009). This indicates that PD patient carriers of more variants in the *SNCA* gene had also been exposed more often to these two pesticides than expected i.e. the risk of PD in this group of patients reflects both their genetic susceptibility and higher levels of Dicamba exposure. The *GBA* SNP-set showed evidence of interaction with 14 pesticides, including MCPA (p=7.35e-04) and dinoseb (p=3.91e-05), with the burden of rare variants being more important than the common variants. We know that some of these pesticides are correlated, as they are often either co-applied or applied sequentially across different seasons on the same fields. We handle this correlated-ness in two ways in the GxE analysis, first assessing orthogonal hierarchical exposure clusters we built, and second using single pesticides and mixtures in the in-vitro cell lines, to pinpoint whether toxicity is due to a single pesticide driving the results or whether the mixture of pesticide exposures is most harmful.

In a future phase of this research, we will use validated hits from the lab-based screens to assess interactions with pathways of relevance and known functional SNPs in additional GxE analyses.

Finally, based on a broad drug screen we conducted in our SNCA h-iPS cells (see above), we selected a KEGG pathway that was implicated by multiple compound hits and that is relevant to PD etiology due to its importance for neuroinflammation i.e. the Nuclear factor kappa B (NF-κB) pathway. The NF-κB pathway includes a family of inducible transcription factors expressed in various cells and tissues (Singh, S.S., Rai, S.N., Birla, H. *et al.* NF-κB-Mediated Neuroinflammation in Parkinson's Disease and Potential Therapeutic Effect of Polyphenols. *Neurotox Res* 37, 491–507 (2020). https://doi.org/10.1007/s12640-019-00147-2). It is a crucial mediator of inflammatory reactions controlling numerous facets of innate and adaptive immune processes (Liu, T., Zhang, L., Joo, D. *et al.* NF-κB signaling in inflammation. *Sig Transduct Target Ther* 2, 17023 (2017). https://doi.org/10.1038/sigtrans.2017.23). Specifically, we identified 104 genes in the NF-κB pathway from the KEGG Pathway database and performed a SKAT summary analysis for all genes in this pathway in the PEG population. **Figure 31** displays all 104 genes in the NF-κB pathway. We removed IGH-(immunoglobulin heavy variable 4-38-2-like) and CCL4L1 as their specific locations on reference GRCh37.p13 were unavailable. We filtered our data with PLINK2, skipped variants whose GT field was absent, excluded all variants with one or more multi-character allele code, and those with a Hardy-Weinberg equilibrium exact test p-value <1e-7. A total of 51,3465 variants passed filtering and quality control in all PEG participants. We then restricted the data to SNPs within the range of the 102 genes in the NF-κB pathway and a total of 1,098 variants remained for testing with the SNP-set (Sequence) Kernel Association Test (SKAT). We conducted SKAT analyses with a linear weighted kernel to account for rarer variants with larger effect sizes being more likely causal. Employing the general SKAT, for an initial 1,621 subjects with sufficient data for analysis we calculated a p-value of 0.1615. Further restricting to 1,506 PEG subjects with complete data we got a p-value of 0.077. Thus, for all variants in the 102 genes in the NF-kB pathway combined, we found only suggestive evidence for a genetic association with PD. However, we are planning in the future, to explore potential GxE interactions for NF-κB pathway variants and the pesticides we identified as related to PD risk in a similar manner as described above for the well-known PD risk genes *SNCA* and *GBA*.

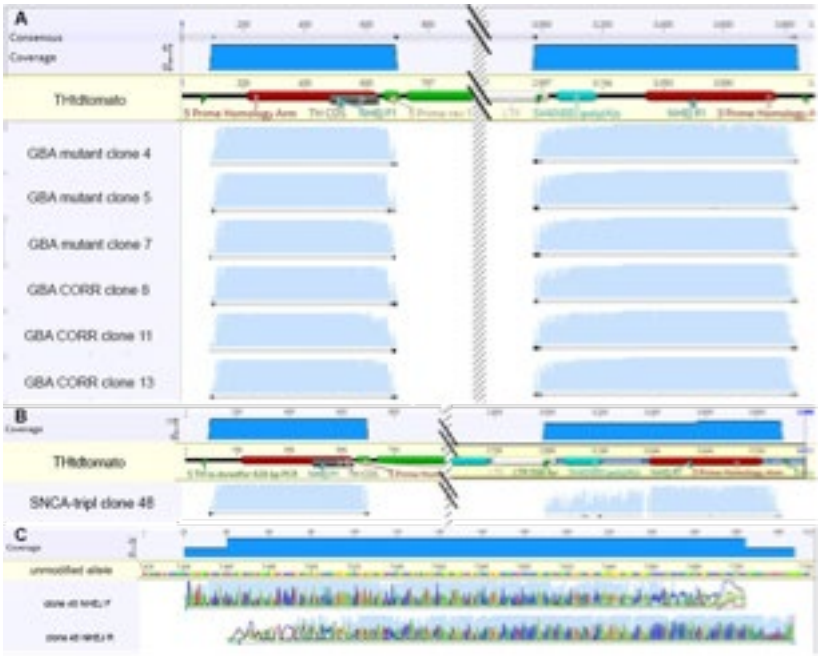

Figure 1. GBA sequence alignment of each clone at 5 prime and 3 prime insertion sites mapped to expected sequence of TH:tdtomato knock in sequence. Crosshatched region represents cropped sequence within the reporter for ease of visualization. **B.** Sequence alignment of SNCA-tripl THtdtomato knock in clone 48. Sequence alignment of additional clones omitted for simplicity. Upper panel shows a cropped version of the expected THtdtomato knock in allele with Sanger sequencing of PCR products from clone 48 demonstrating proper insertion at the 5 prime and 3 prime ends of the reporter construct. **C.** Integrity of the unmodified allele of TH in the region of the CRISPR-targeted sequence.

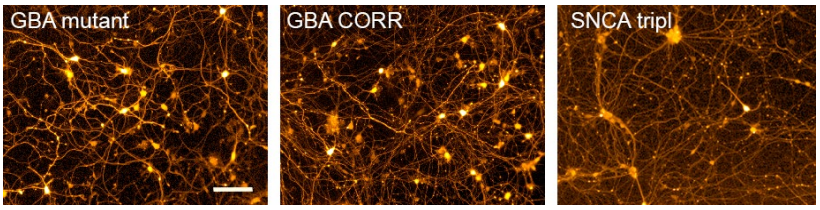

Figure 2: Live cell imaging of endogenous reporter fluorescence for GBA mutant TH:tdtomato knock in (left panel), isogenic corrected control GBA line with TH:tdtomato knock in (center panel), and SNCA triplication TH:tdtomato knock in (right panel). Images acquired with Molecular devices IXM high content imaging system with 10x objective. Scale bar 100uM.

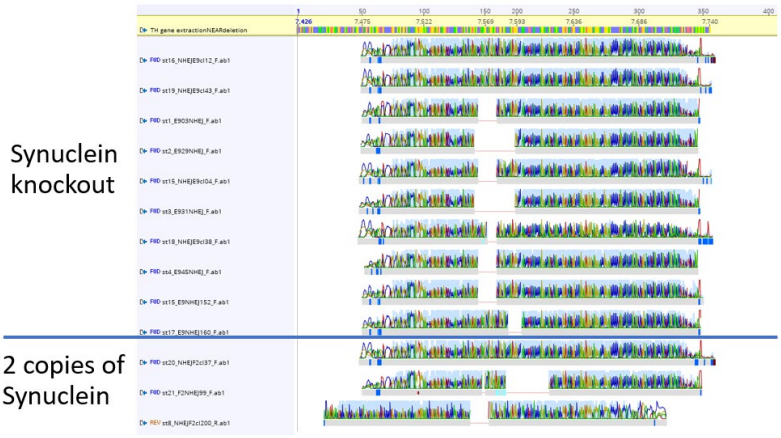

Figure 3. Sequence alignment of each clone at unmodified TH allele demonstrating substantial NHEJ error prevalence in synuclein knockout and knockdown lines. First two lines listed passed all PCR and differentiation quality control criteria. Clone 43 has a normal karyotype and is used for experiments going forward.

SNCA-triplication	EC50 values in µM **condition**	
Toxicant	sorted	mixed
Rotenone	0.025	0.043
Cyanazine	696	574
Permethrin	21.4	22
Paraquat	5	ND (>30)

Table 1. SNCA triplication toxicant sensitivity assay comparison: sorted vs mixed samples. EC50 represents the value at which 50% of the maximum cell death occurred. EC50 values were calculated using a Smart Fit algorithm in GeneData software. Experiment was performed as a 6 concentration dose curve in triplicate.

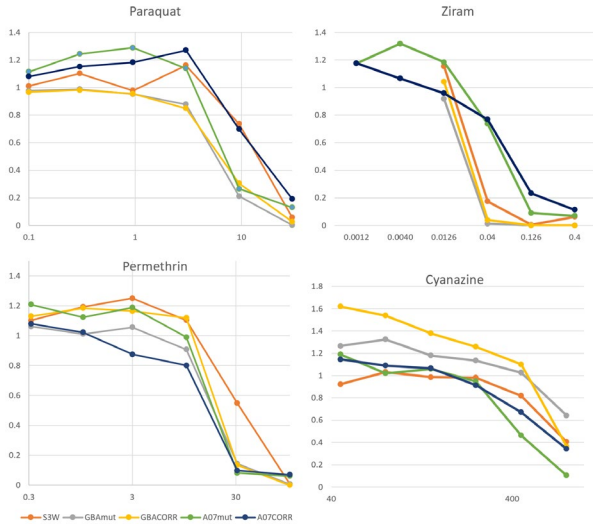

Figure 4. FACS purified THtd+ neurons from the SNCA-tripl (“S3W”), GBA mutant (“GBAmut”), GBA corrected (“GBACORR”), E46K mutant (“A07mut”) and E46K corrected (“A07CORR”) cell lines were treated with multiple doses of toxicants (x-axis in micromolar) linked to PD risk. Cell numbers measured by high content imaging of live cultures 11 days after first treatment and normalized to DMSO control for each line (y axis).

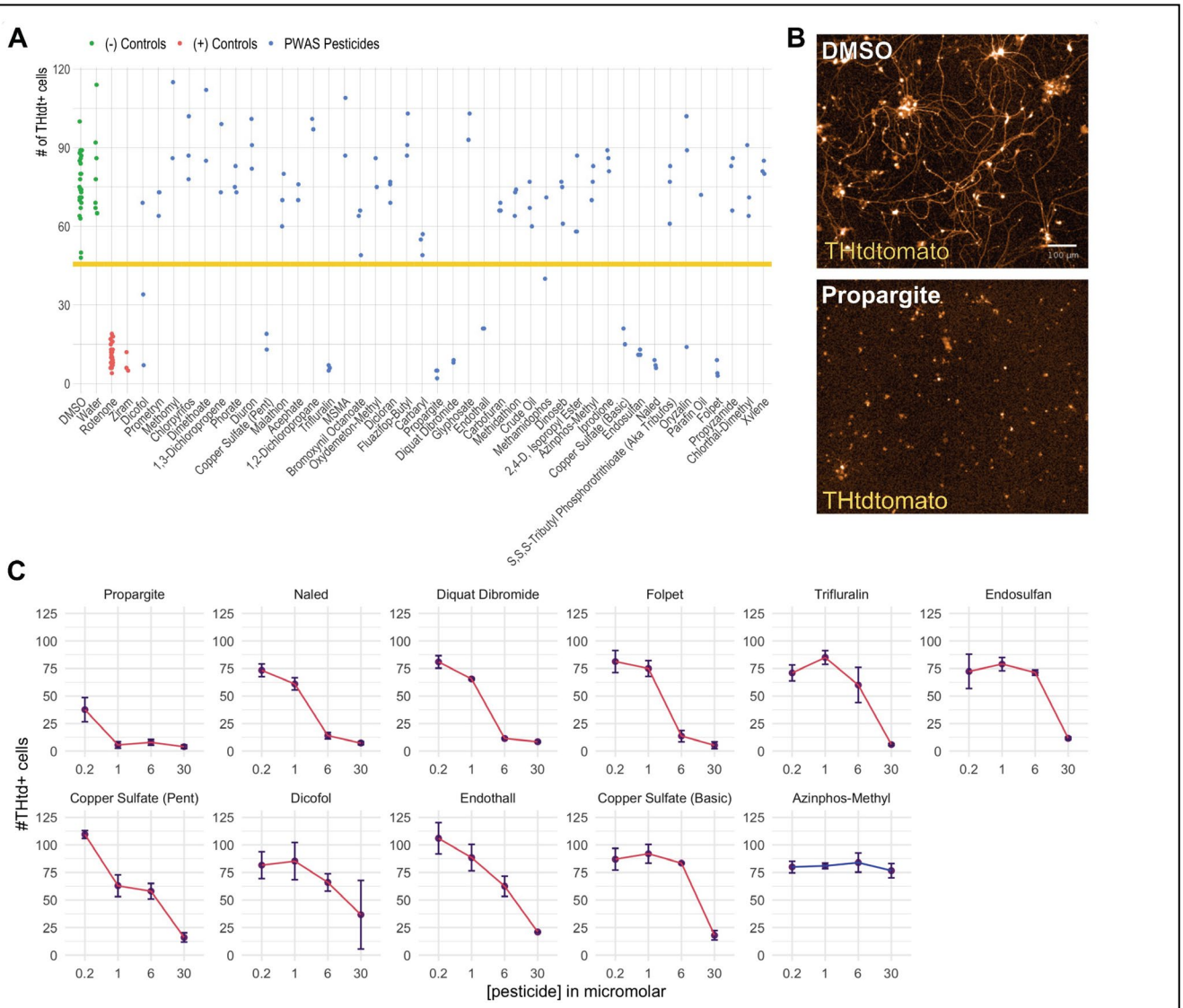

Figure 5. PWAS pesticides are directly toxic to mDA neurons

(A) Scatter plot with the number of THtdTomato+ cells measured by live imaging analysis 11 days after the first treatment. DMSO controls (green data points) were present on each assay plate. Water control (light blue) was present on the assay plate containing primarily water-soluble pesticides. Rotenone (red data points) and ziram (purple data point) were used as positive controls. Blue data points represent the different pesticides from the PWAS study. Horizontal line denotes three standard deviations below DMSO mean. **(B)** Upper image is a 10x magnification live image of a DMSO control well. Lower image is from a propargite well. Scale bar = 100µM. **(C)** Four concentration dose curves of PWAS toxicants producing death in SNCA triplication THtdTomato sorted neurons. Cell numbers measured by high content imaging of live cultures 11 days after first treatment. Error bars are two standard deviations (one above, one below).

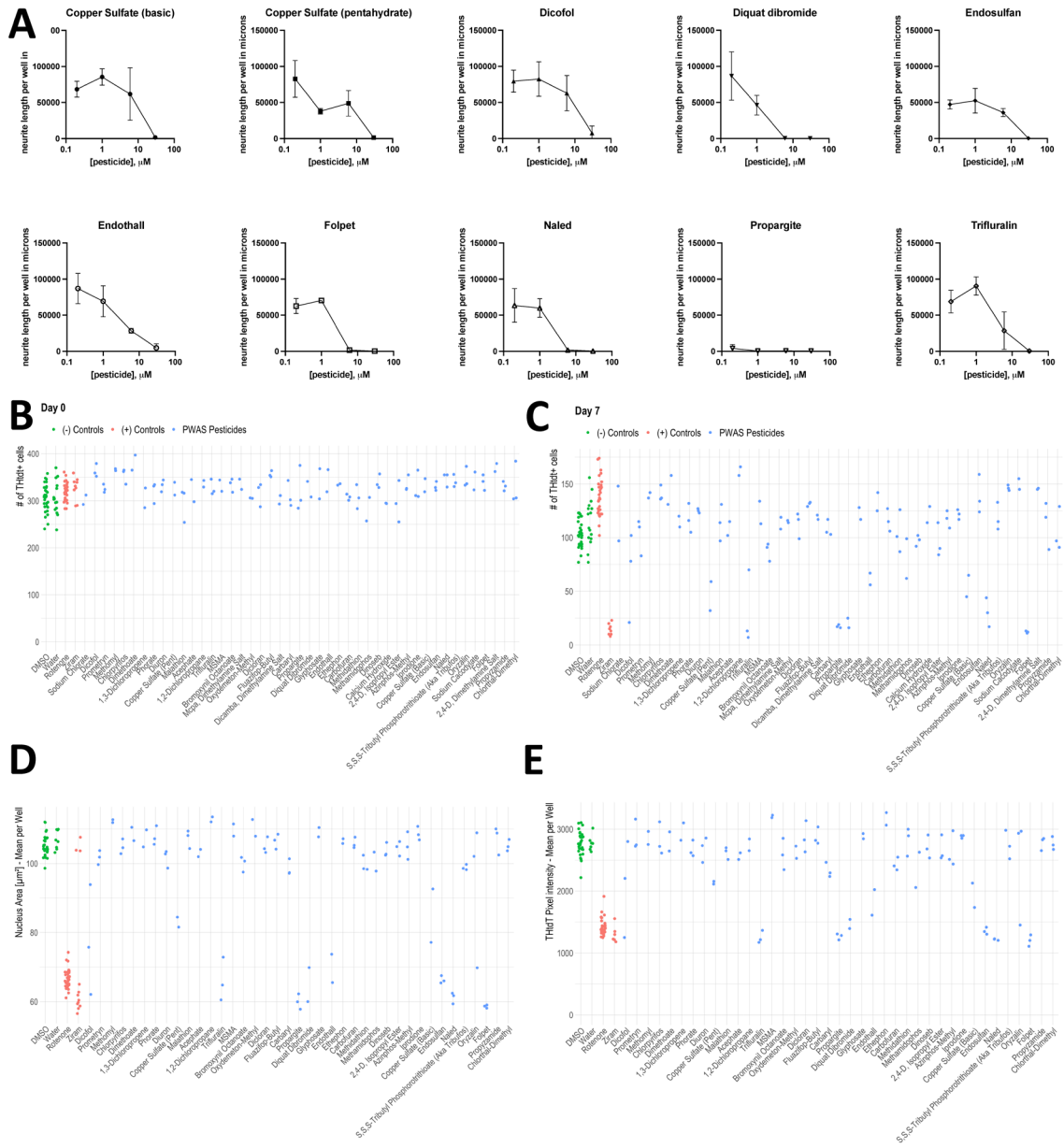

Figure 6. Detailed morphometric data from live-imaging PWAS screen. A. Dose response curves of neurite length (y-axis) for each of the ten toxic PWAS pesticides. B,C. Scatter plots of mDA neuron cell counts are provided for pre-treatment (day 0) and day 7 post treatment. In B, the conditions labelled on the x-axis represent the wells that have not yet been exposed to the pesticides listed. D. Cell area measurements for the entire set of screened PWAS pesticides. THtdT reporter signal was measured in the cell body excluding signal in the neurites. E. Average THtdT signal intensity in each pesticide condition.

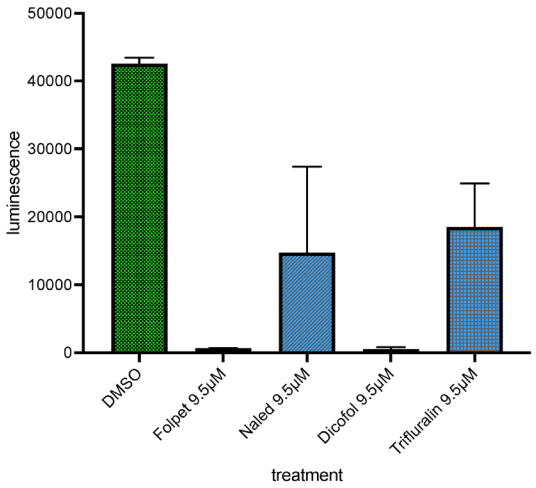

Figure 7. Cell viability as assessed by CellTitre-Glo based ATP measurement. The subset of toxic pesticides that are DMSO-soluble were retested in the SNCA triplication THtdT mDA neurons using the CellTitre-Glo assay (Promega) as a readout of remaining viable cells. All four pesticides resulted in the expected reduction of viable cells at or below the original screening concentration as measured by CellTitre-Glo assay at 11 days post pesticide treatment. Average and standard deviation of 2-3 technical replicates from a single experiment are shown.

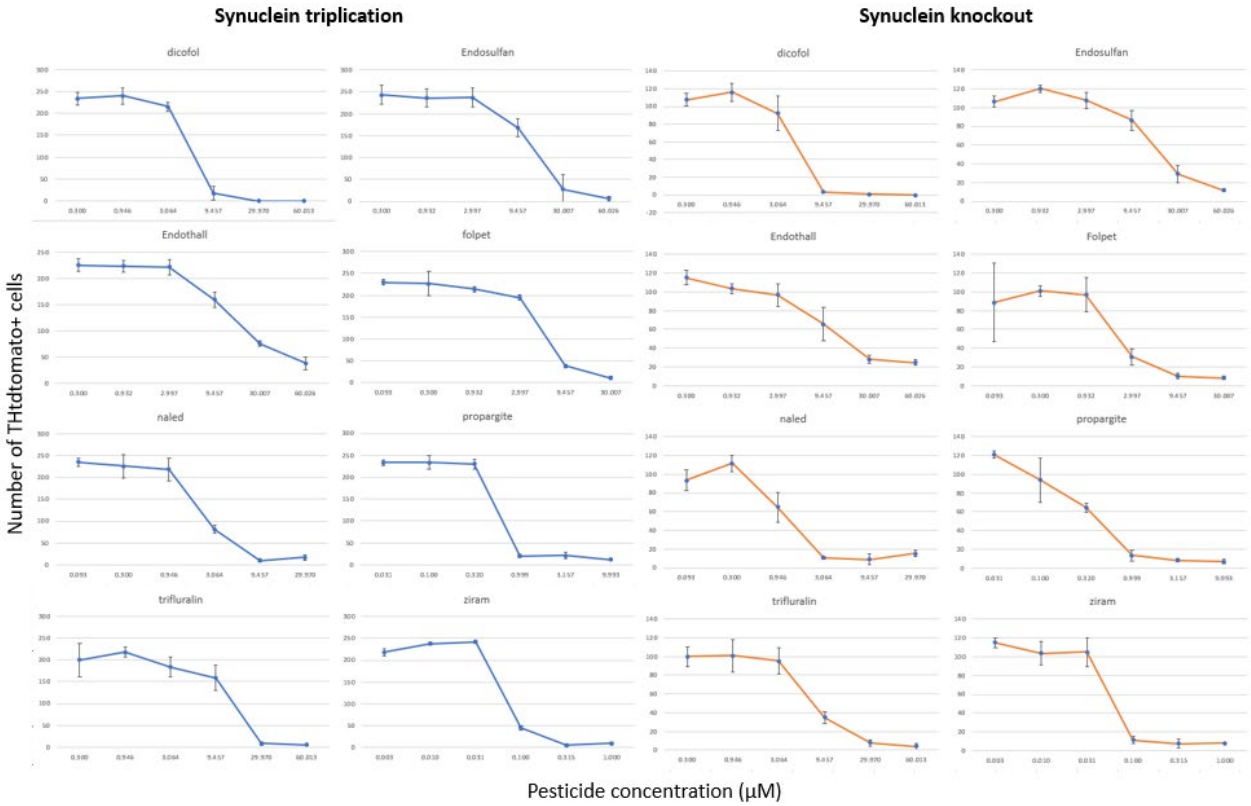

Figure 8: Sensitivity of dopaminergic neurons from synuclein triplication and synuclein knockout isogenic lines to PEG/PWAS pesticides. Y-axis is raw counts of cell numbers with error bars showing +/- one standard deviation. Concentration on x-axis in micromolar

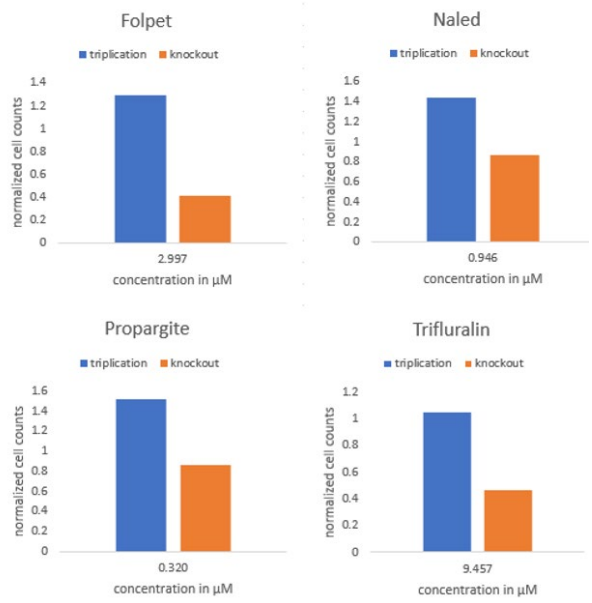

Figure 9: Normalized cell counts for direct comparison of sensitivity to pesticides for synuclein triplication and synuclein knockout dopaminergic neurons. Data highlights the dose at which the largest difference between triplication and knockout was observed.

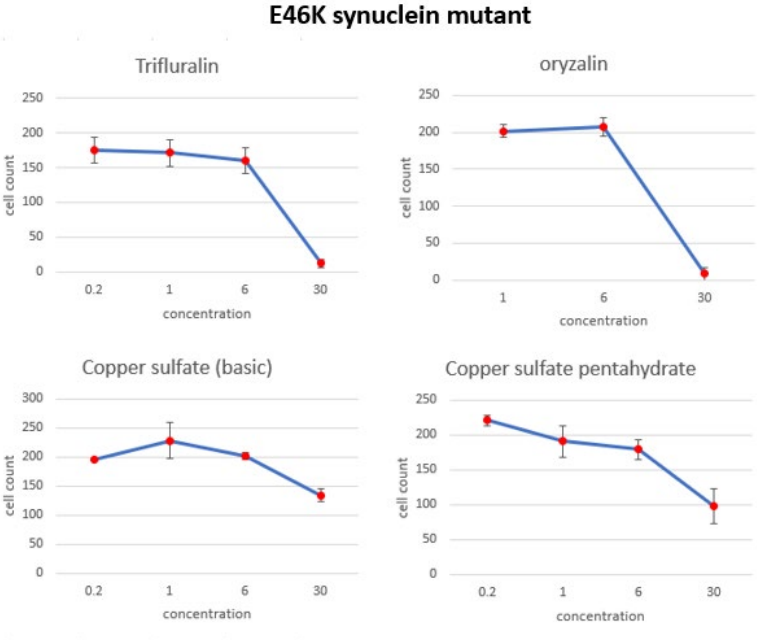

Figure 10: Sensitivity of E46K synuclein mutant dopaminergic neurons to select PEG/PWAS pesticides

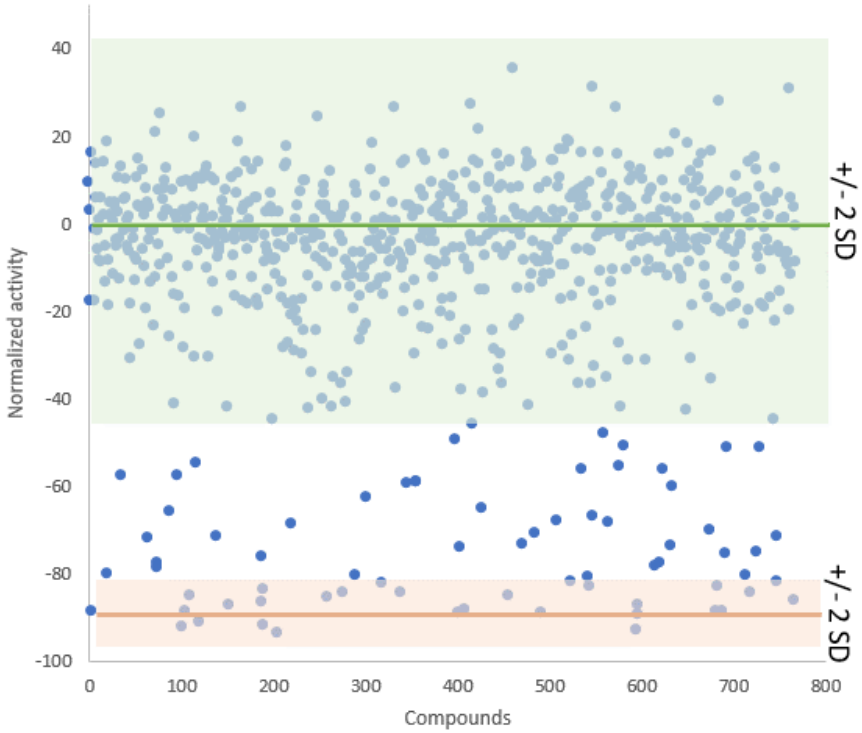

Figure 11. Scatter plot of normalized compound screen result. Green shaded area is two standard deviations above and below the DMSO control. Orange shaded area is two standard deviations above and below the positive control, Berzosertib, which had an activity of -89.6. Standard deviation of DMSO control is 22.3. Seventy compounds had activity <-44.9 (2SD below control) and fifty-two compounds had activity <-66.9 (3SD below control).

Compound ID	Activity17	Target	Information	Pathway
Ciclopirox ethanolamine	-93.732758	ATPase	Ciclopirox ethanolamine (Ciclopirox olamine, HOE 296) is a broad-spectrur	Transmembrane Transporters
Pyrrolidinedithiocarbamate ammonium	-92.694618	NF-κB	Ammonium pyrrolidine dithiocarbamate (PDTC) is a potent inhibitor of nuc	NF-κB
b-AP15	-92.313362	DUB	b-AP15 is a deubiquitinases inhibitor for 19S proteasomes activity of Ub-Al	Ubiquitin
Chlorhexidine 2HCl	-91.716652	Antifection	Chlorhexidine hydrochloride is an antiseptic effective against a wide varie	Others
Berbamine (dihydrochloride)	-91.011749	Bcr-Abl	Berbamine (BBM) is a natural bisbenzylisoquinoline product isolated from	Angiogenesis
Quinacrine 2HCl	-89.505966	Phospholipase (e.g. PLA)	Quinacrine 2HCl is a lipophilic cationic drug with multiple actions that is co	Others
IKK-16 (IKK Inhibitor VII)	-89.079231	IκB/IKK	IKK-16 (IKK Inhibitor VII) is a selective IκB kinase (IKK) inhibitor for IKK-2, IKK	NF-κB
Moxidectin	-88.812286	Antifection	Moxidectin is a potent, broad-spectrum endectocide with activity against	Microbiology
Thimerosal	-88.595421	Antifection	Thimerosal is a well-established antiseptic and antifungal agent and usua	Microbiology
Beclomethasone dipropionate	-88.526276	Glucocorticoid Receptor	Beclomethasone dipropionate is a potent glucocorticoid steroid used for t	Others
(+)-Fangchinoline	-88.484871	Others	Fangchinoline is a phytochemical that has been shown to elicit anti-cance	Others
Tenovin-6	-88.416237	p53,Sirtuin	Tenovin-6 is a small molecule activator of p53 transcriptional activity.	Apoptosis
Isavuconazole	-87.907898	Antifection	Isavuconazole is a new extended-spectrum triazole with activity against ye	Microbiology
QNZ (EVP4593)	-87.422554	NF-κB,TNF-alpha	QNZ (EVP4593) shows potent inhibitory activity toward both NF-κB activati	NF-κB
Cabozantinib malate (XL184)	-87.135986	TAM Receptor,VEGFR	Cabozantinib malate (XL184) is the malate of Cabozantinib, a potent VEGFF	Protein Tyrosine Kinase
Cepharanthine	-86.52002	TNF-alpha	Cepharanthine is a biscoclaurine alkaloid inhibiting tumor necrosis factor	Others
Zinc Pyrithione	-86.000175	Proton Pump,Antifection	Zinc pyrithione is an antifungal and antibacterial agent disrupting membra	Transmembrane Transporters
DHBP dibromide	-85.667145	Calcium Channel	DHBP, a viologen for electrochromic memory display agent, inhibits the ca	Transmembrane Transporters
Mefloquine HCl	-85.170624	Antifection	Mefloquine HCl is a blood schizonticide by inhibiting hemozoin formation,	Others
Benzethonium Chloride	-85.134384	AChR	Benzethonium chloride is a potent inhibitor of nAChRs, it inhibits α4β2 nAC	Others
Fangchinoline	-84.395454	Reverse Transcriptase	Fangchinoline, a bisbenzylisoquinoline alkaloid, is a novel HIV-1 inhibitor v	Microbiology
Triptolide (PG490)	-84.267509	NF-κB	Triptolide is a diterpene triepoxide, immunosuppresive agent extracted fr	Others
Digoxin	-84.113976	Sodium Channel	Digoxin is a classical Na,K-ATPase inhibitor, with selectivity for the α2β3 is	Transmembrane Transporters
Cetylpyridinium Chloride	-83.422546	Antifection	Cetylpyridinium chloride is a cationic quaternary ammonium compound us	Others
Terfenadine	-83.129807	Others	Terfenadine is an antihistamine, generally completely metabolizes to the	Others
Pentamidine isethionate	-82.797729	phosphatase	Pentamidine is an inhibitor of PRL Phosphatases and also inhibits synthes	Others
Ethacridine lactate monohydrate	-82.073158	Antifection	Ethacridine lactate monohydrate is an aromatic organic compound based	Others
Vinorelbine Tartrate	-81.855698	Microtubule Associated	Vinorelbine Tartrate is a semi-synthetic vinca alkaloid, and inhibits mitosi	Cytoskeletal Signaling
Ouabain	-81.740135	Sodium Channel	Ouabain is a selective Na+/K+, -ATPase inhibitor, binds to α2 /α3 subunit w	Transmembrane Transporters
Penfluridol	-80.726555	Dopamine Receptor	Penfluridol is a highly potent, first generation diphenylbutylpiperidine ant	Others
Trifluoperazine 2HCl	-80.619713	Dopamine Receptor	Trifluoperazine is a dopamine D2 receptor inhibitor with IC50 of 1.1 nM.	Ubiquitin
Domiphen Bromide	-80.397568	Others	Domiphen bromide is a quaternary ammonium antiseptic with actions as a	Others
2-Methoxy-1,4-naphthoquinone	-79.938271	PKC	2-Methoxy-1,4-naphthoquinone, isolated from the leaves of Impatiens gla	Cytoskeletal Signaling
Arctiin	-78.722435	Opioid Receptor	Arctiin acts on an agonists of the adiponectin receptor 1 with anti-cancer e	Others
Ropinirole HCl	-78.178589	Dopamine Receptor	Ropinirole a selective dopamine D2 receptors agonist with Ki of 29 nM.	Others
Salmeterol Xinafoate	-77.520355	Adrenergic Receptor	Salmeterol Xinafoate is a long-acting β2-adrenergic receptor agonist with a	GPCR & G Protein
Apoptosis Activator 2	-77.438316	Caspase	Apoptosis Activator 2 strongly induces caspase-3 activation, PARP cleavag	Apoptosis
Cetrimonium Bromide (CTAB)	-76.246231	Antifection	Cetrimonium Bromide is a known component of the broad-spectrum antise	Others
Thioridazine HCl	-75.186798	Others	Thioridazine is a trifluoro-methyl phenothiazine derivative, which blocks p	Others
Tulathromycin A	-74.885002	Others	Tulathromycin A is a novel long-acting semi-synthetic tribasic macyocyclic	Others
IMD 0354	-74.119423	IκB/IKK	IMD-0354 is an IKKβ inhibitor and blocks IκBα phosphorylation in NF-κB pat	NF-κB
Sertaconazole nitrate	-73.522911	Antifection	Sertaconazole nitrate is a topical broad-spectrum antifungal that is develc	Others
Methylene Blue	-73.399696	Others	Methylene Blue is used as a dye in chromoendoscopy. It Inhibits tau filame	Others
Amodiaquine dihydrochloride dihydrate	-72.147591	Transferase,Histone Methyltra	Amodiaquine is a potent, non-competitive inhibitor of histamine N-methyl	Others
Vinblastine sulfate	-71.654404	Microtubule Associated,AChR	Vinblastine sulfate inhibits microtubule formation and suppresses nAChR	Cytoskeletal Signaling
Brexpiprazole	-71.382271	5-HT Receptor,Dopamine Rece	Brexpiprazole is a novel D2 dopamine and serotonin 1A partial agonist, cal	Neuronal Signaling
MLN0905	-70.533165	PLK	MLN0905 is a potent inhibitor of PLK1 with IC50 of 2 nM.	Cell Cycle
Tazobactam	-69.708168	Antifection	Tazobactam is a β-lactamases Inhibitor with antibacterial activity. It also i	Others
Clofoctol	-68.595963	Others	0	Others
Pimozide	-68.191704	Others	Pimozide is an antipsychotic drug of the diphenylbutylpiperidine class, wh	Others
Nifuroxazide	-67.539307	STAT	Nifuroxazide is a cell-permeable and orally available nitrofuran-based ant	Others
Perphenazine	-67.078995	Dopamine Receptor	Perphenazine is a phenothiazine derivative and a dopamine antagonist wi	Neuronal Signaling

Table 2: Screen results from synuclein triplication toxicity screen. The compounds resulting in cell death >3 standard deviations greater than the DMSO control wells and their corresponding annotations provided by the commercial vendor are listed. More negative "Activity" values indicate conditions with less surviving THtdtomato + neurons

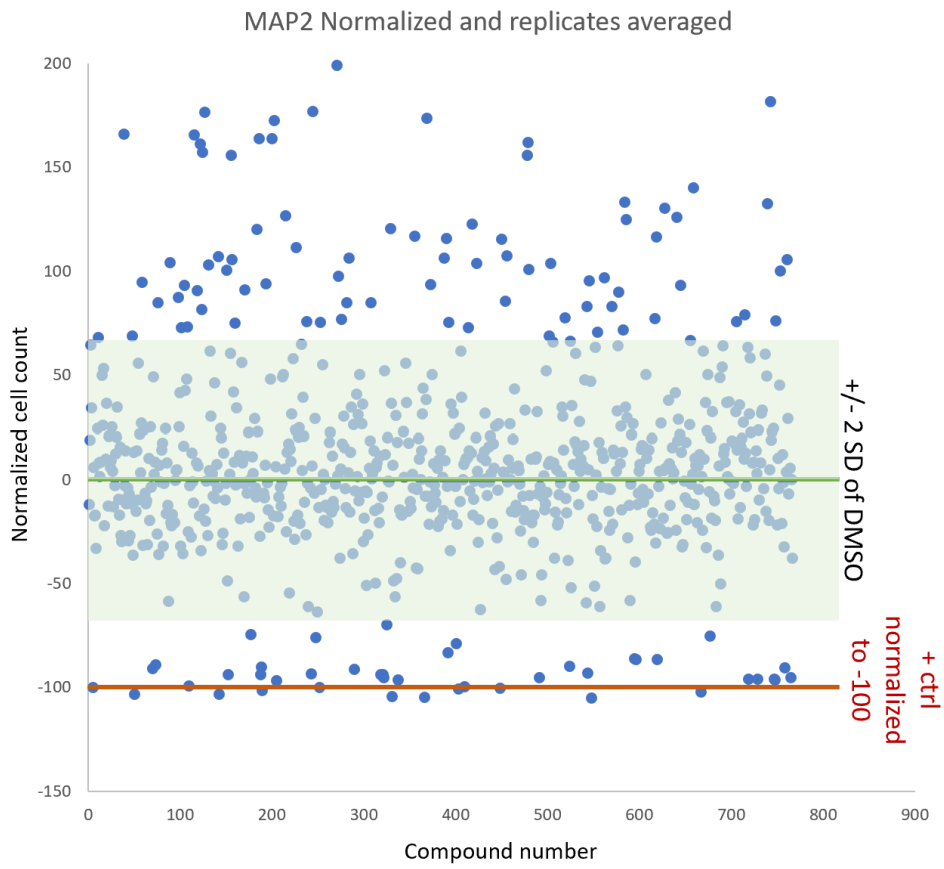

Figure 12: Scatter plot of iNGN cortical neuron counter screen. Y-axis is cell count as determined by MAP2 positivity in the perinuclear cytoplasm, normalized to DMSO negative control and Berzosertib positive control (scaled to -100; red line). X axis is the compounds. Green box represents two standard deviations above and below the negative control (DMSO normalized mean). Compounds two standard deviations below the DMSO mean were considered toxic. Normalization and analysis performed with GeneData Screener analysis software.

DA neuron hits 48 unique to DANs				
Compound ID	DA neuron Activity	iNGN activity	Target	Pathway
Mefloquine HCl	-98.61	-47.99	Antifection	Others
b-AP15	-98.41	-32.02	DUB	Ubiquitin
Berbamine (dihydrochloride)	-98.36	-17.72	Bcr-Abl	NFkB/Angiogenesis
Beclomethasone dipropionate	-98.22	15.88	Glucocorticoid Receptor	Others
Arctiin	-98.08	-26.45	Opioid Receptor	Others
DHBP dibromide	-97.98	-20.85	Calcium Channel	Transmembrane Transporters
Tenovin-6	-97.96	-10.22	p53,Sirtuin	Apoptosis
QNZ (EVP4593)	-97.87	-39.77	NF-κB,TNF-alpha	NF-?B
Penfluridol	-97.76	-59.29	Dopamine Receptor	Others
Flupenthixol dihydrochloride	-97.62	116.48	Dopamine Receptor,Adrenergic Receptor	Neuronal Signaling
Thioridazine HCl	-97.52	63.94	Dopamine Receptor	Neuronal Signaling
Brexpiprazole	-97.51	-9.27	5-HT Receptor,Dopamine Receptor	Neuronal Signaling
Amodiaquine dihydrochloride dihydrat	-97.47	-31.41	Transferase,Histone Methyltransferase	Others
Pimozide	-97.41	-37.80	Others	Neuronal Signaling/Antipsychotic
Methylene Blue	-97.14	-46.09	Others	Others
Trifluoperazine 2HCl	-97.13	27.23	Dopamine Receptor	Neuronal Signaling
Thimerosal	-97.10	-50.50	Antifection	Microbiology
Lercanidipine hydrochloride	-96.91	-62.59	Calcium Channel	Transmembrane Transporters
Ifenprodil Tartrate	-96.88	21.60	NMDAR	Neuronal Signaling
Cepharanthine	-96.87	-27.46	TNF-alpha	NFkB
Terfenadine	-96.25	-61.34	Others	Others
Salmeterol Xinafoate	-96.08	-3.47	Adrenergic Receptor	GPCR & G Protein
Digoxin	-95.86	76.79	Sodium Channel	Transmembrane Transporters
JNK-IN-8	-95.69	122.51	JNK	MAPK
Fluphenazine dihydrochloride	-95.62	-42.83	Dopamine Receptor	GPCR & G Protein
Ropinirole HCl	-95.55	19.54	Dopamine Receptor	Others
Tazobactam	-95.09	-5.97	Antifection	Others
Tulathromycin A	-94.71	8.25	Others	Others
Clofoctol	-94.70	-54.61	Others	Others
Sertraline HCl	-94.39	-12.59	5-HT Receptor	Neuronal Signaling
Sertaconazole nitrate	-93.62	7.64	Antifection	Others
2-Methoxy-1,4-naphthoquinone	-93.56	316.44	PKC	Cytoskeletal Signaling
ELR-510444	-93.43	-51.20	Microtubule Associated	Cytoskeletal Signaling
Prochlorperazine dimaleate salt	-93.42	12.88	Dopamine Receptor	Neuronal Signaling
MLN0905	-93.15	-30.30	PLK	Cell Cycle
9-Aminoacridine	-93.06	-27.14	Others	Others
Fingolimod (FTY720) HCl	-91.28	55.70	S1P Receptor	GPCR & G Protein
Azaguanine-8	-90.22	-58.85	Others	Others
Sarpogrelate hydrochloride	-89.95	26.79	5-HT Receptor	Neuronal Signaling
Benzydamine HCl	-89.65	165.52	Immunology & Inflammation related	Others
Nifuroxazide	-87.09	-38.10	STAT	Others
Paroxetine HCl	-86.32	9.56	AChR,5-HT Receptor	Neuronal Signaling
Vilanterol Trifenate	-85.48	18.82	Adrenergic Receptor	Neuronal Signaling
Tilmicosin	-84.52	8.13	Antifection	Others
Azithromycin Dihydrate	-83.77	4.21	Antifection	Others
Primaquine Diphosphate	-82.32	64.07	Antifection	Others
Chlorquinaldol	-66.55	47.98	Antifection	Others
Pifithrin-μ	-60.38	10.20	p53	Apoptosis

Table 3: Compounds called as hits in the dopaminergic neuron screen that were not called as hits in the iNGN screen. Activity of -100 is maximal, DMSO negative control scaled to zero activity. Positive activity values for iNGN column indicates increased cell counts as measured by MAP2 staining compared to DMSO control.

DA neuron and iNGN hits 25 shared				
Compound ID	DA neuron Activity	iNGN activity	Target	Pathway
Cetylpyridinium Chloride	-99.06	-90.32	Antifection	Others
Isavuconazole	-98.88	-99.68	Antifection	Microbiology
Cetrimonium Bromide (CTAB)	-98.72	-93.95	Antifection	Others
Fangchinoline	-98.50	-96.68	Reverse Transcriptase	Microbiology
Benzethonium Chloride	-98.48	-99.54	AChR	Others
Zinc Pyrithione	-98.30	-95.30	Proton Pump,Antifection	Transmembrane Transporters
IMD 0354	-98.28	-101.03	IκB/IKK	NF-κB
Quinacrine 2HCl	-98.26	-86.69	Phospholipase (e.g. PLA)	Others
Triptolide (PG490)	-98.22	-96.29	NF-κB	Others
Domiphen Bromide	-98.16	-91.44	Others	Others
Pentamidine isethionate	-98.06	-93.10	phosphatase	Others
Pyrrolidinedithiocarbamate ammonium	-98.05	-86.51	NF-κB	NF-κB
(+)-Fangchinoline	-97.89	-100.17	Others	Others
Ciclopirox ethanolamine	-97.79	-96.94	ATPase	Transmembrane Transporters
Ethacridine lactate monohydrate	-97.72	-94.12	Antifection	Others
Ouabain	-97.68	-89.96	Sodium Channel	Transmembrane Transporters
Cabozantinib malate (XL184)	-97.55	-94.12	TAM Receptor,VEGFR	Protein Tyrosine Kinase
Moxidectin	-97.53	-95.43	Antifection	Microbiology
IKK-16 (IKK Inhibitor VII)	-97.13	-78.91	IκB/IKK	NF-κB
Perphenazine	-97.01	-105.41	Dopamine Receptor	Neuronal Signaling
Vinblastine sulfate	-96.36	-96.22	Microtubule Associated,AChR	Cytoskeletal Signaling
Vinorelbine Tartrate	-95.17	-96.62	Microtubule Associated	Cytoskeletal Signaling
Apoptosis Activator 2	-93.41	-89.21	Caspase	Apoptosis
Tyrphostin 9	-74.95	-96.03	PDGFR,EGFR	Protein Tyrosine Kinase
Chlorhexidine 2HCl	-97.16	-101.48	Antifection	Others

Table 4: Compounds called as hits in the dopaminergic neuron screen that were also called as hits in the iNGN screen. Activity of -100 is maximal, DMSO negative control scaled to zero activity. Dopaminergic neuron (DA) values provided alongside iNGN cortical neuron values for comparison.

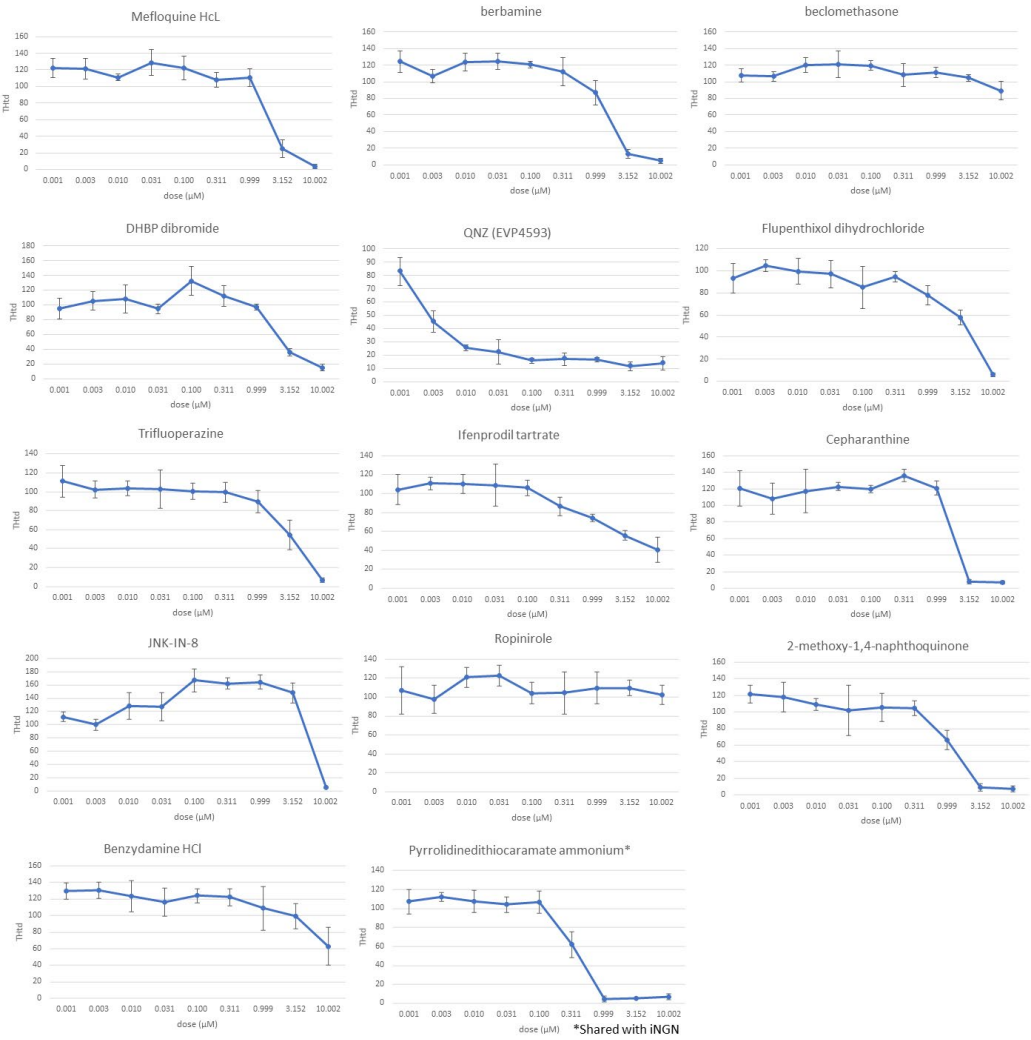

Figure 13: Nine concentration dose curve validation on synuclein triplication THtdtomato+ dopaminergic neurons for selected hits from the SelleckChem dopaminergic neuron screen. Number of THtd+ neurons on y axis, compound concentration on x-axis.

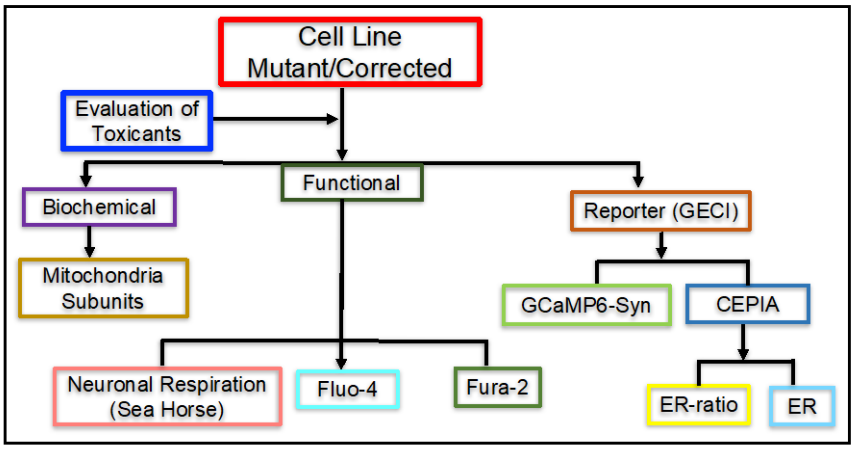

Figure 14. Neuronal functionality assay toolbox at Khurana Lab

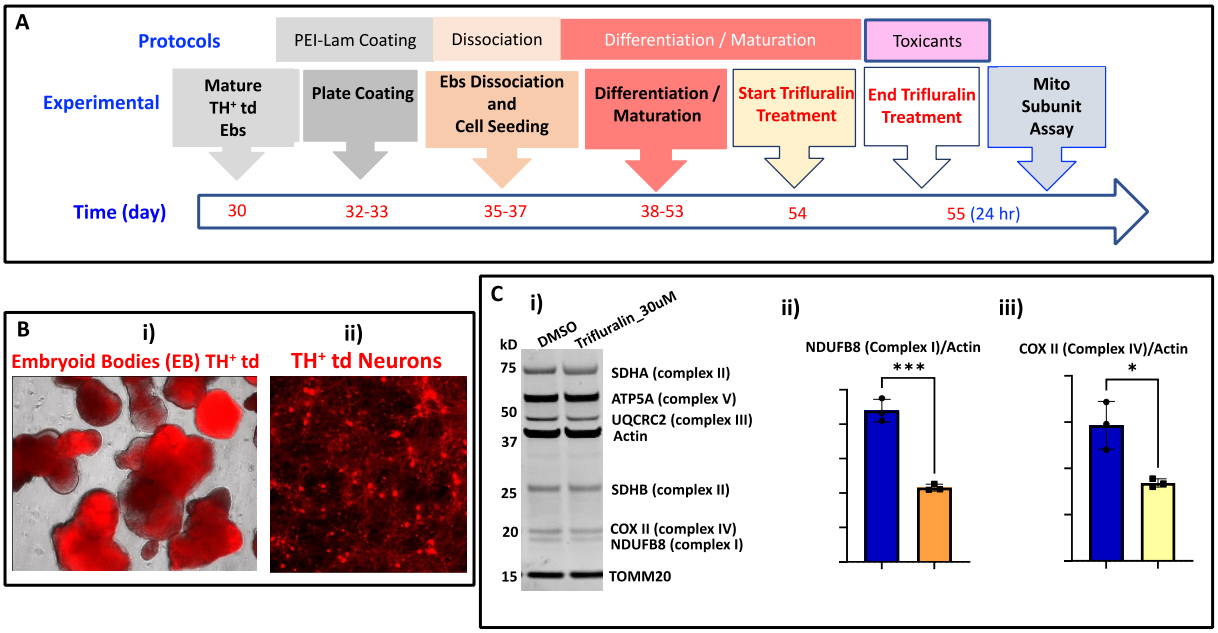

Figure 15. Mitochondria subunit assay and effect of Trifluralin. A) work-flow of mitochondria subunit assay using trifluralin as toxicant. B) Picture of TH^+ td mature embryoid bodies (i) and TH^+ td dissociated neurons (ii). C) Effect of Trifluralin in mitochondria subunits assay, western blot for respiratory chain complexes for differentiated SNC-triplication (S3W) neurons at DIV 65, exposed to 0.3 % DMSO and 30 µM Trifluralin for 24hr (i). Quantification of Complex I (ii) and Complex IV (ii) from blot in (i).

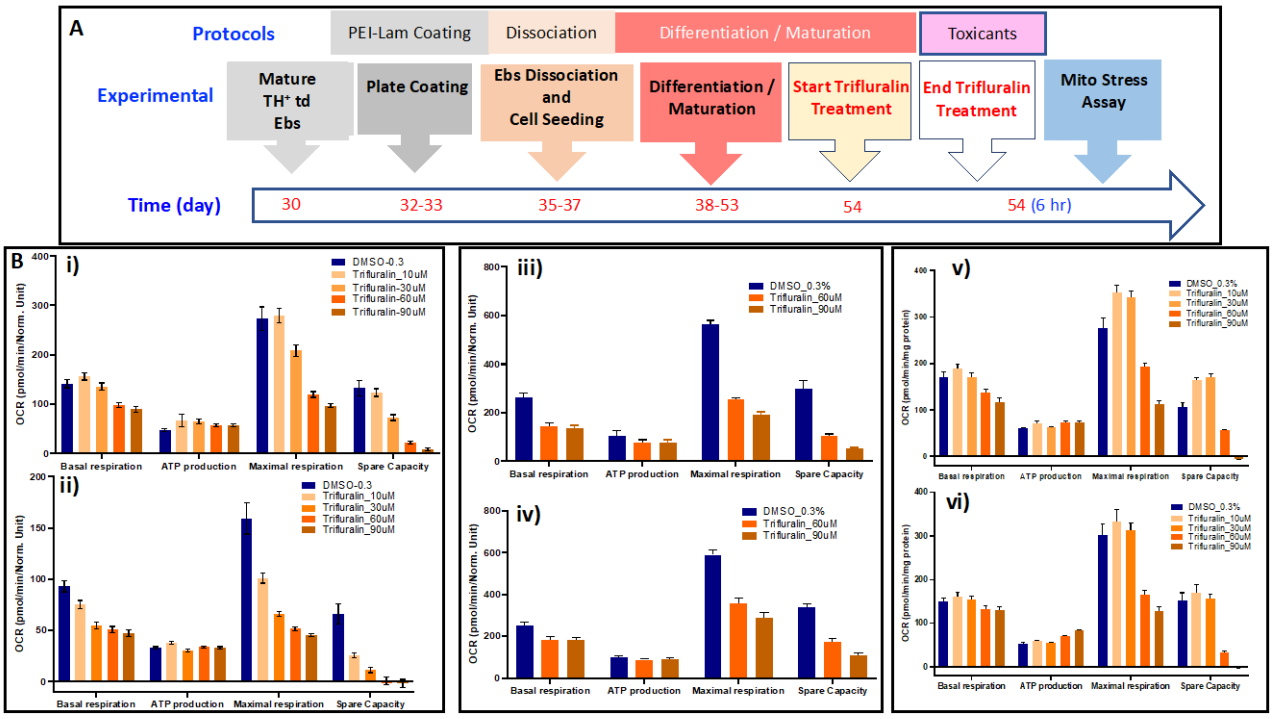

Figure 16. A) work-flow of Neuronal respiration / mito-stress assay using trifluralin as toxicant. B) Measurement of Oxygen Consumption Rate (OCR) and metabolic parameters on Agilent Seahorse XFCell Mito stress assay. Metabolic parameters of dose response effect of DMSO (0.3%) and Trifluralin (10µM, 30µM, 60µM and 90µM) on SNC-triplication (S3W) and SNC-null (E9) (ii) differentiated neurons at DIV 54 and after 6hr exposure. Metabolic parameters for E46K-par1 (A07-mut) (iii) and E46K-Corr (A07-corr) at DMSO (0.3%) and Trifluralin (60µM and 90µM) (iv) and GBA-mut (v) and GBA-corr (iv) differentiated neurons, dose response as in (i).

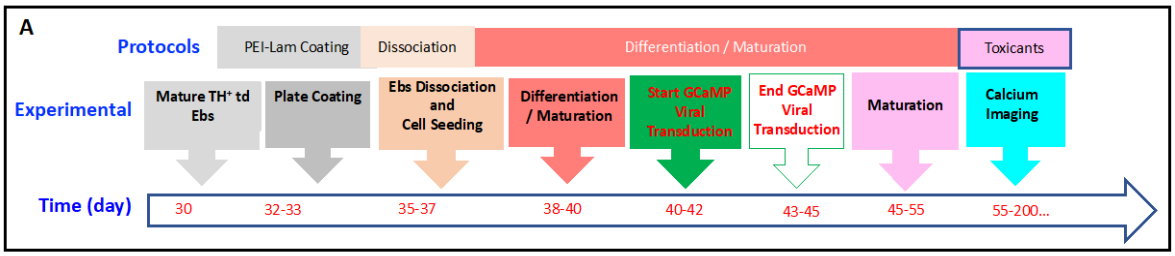

Figure 17. Calcium imaging assay. A) work-flow of Calcium imaging assay using trifluralin as toxicant.

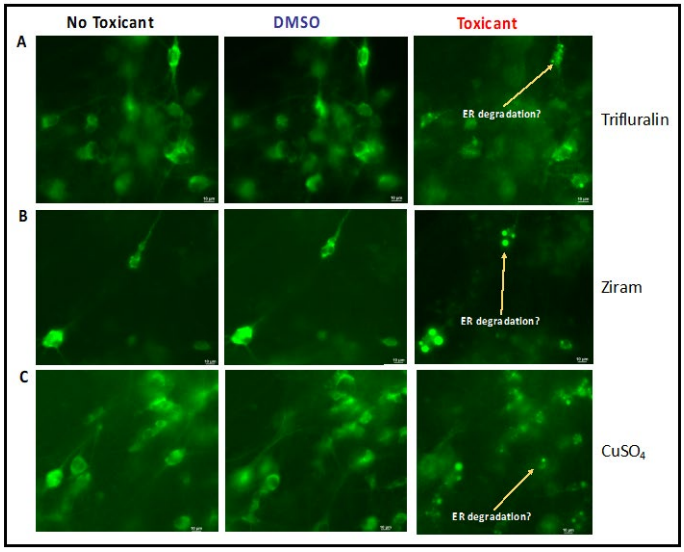

Figure 18. Effect of toxicants on ER of SNCA-triplication (S3W)TH^{+}td differentiated neurons using CEPIA-ER-GFP based calcium imaging assay with, A) no toxicant exposure to DMSO (0.2%) and Trifluralin at 60µM for 6hr, B) Ziram at 1µM for 6hr and C) Copper Sulfate at 60µM for 6hr. The arrows point the formation of intracellular aggregates due to the toxic effect of tested compound.

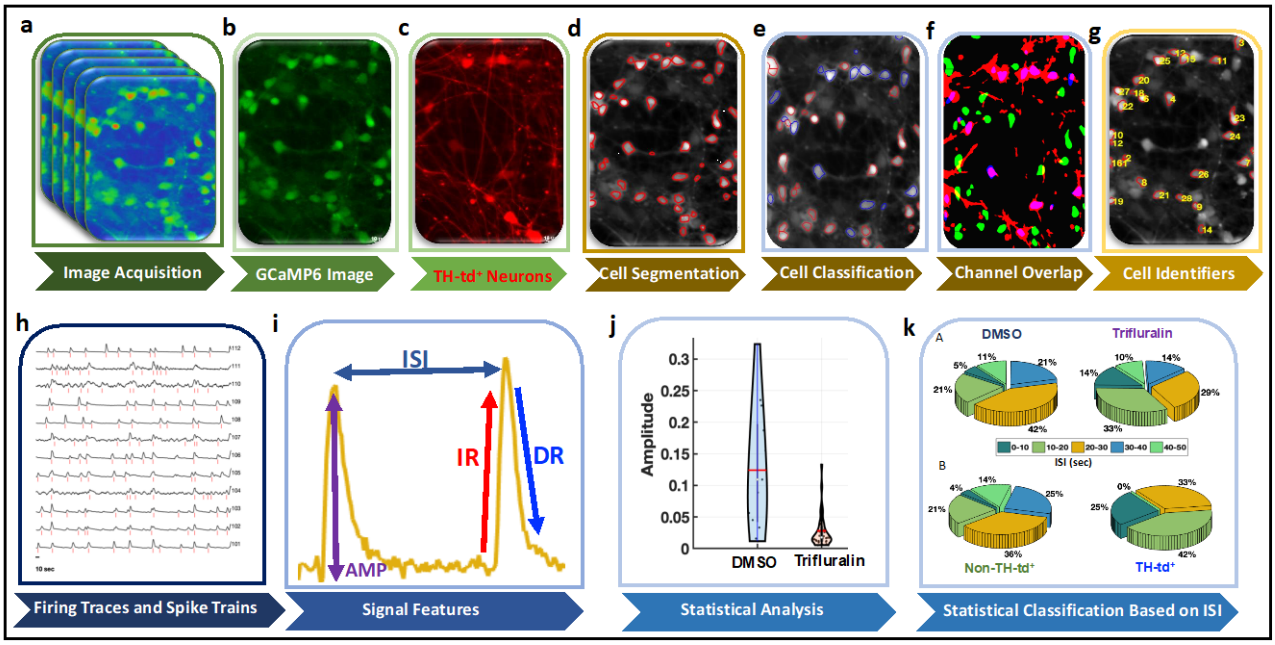

Figure 19.
Automated image analysis pipeline for calcium imaging data analysis to quantify neuronal activity. (a)Time lapse Calcium imaging data of a neuronal population are acquired. (b) GCaMP6 or Fluo-4 are used as calcium indicators. (c) Representative picture of TH-td^{+} neurons. (d) Cells segmentation, (e) Cells classification as TH-td^{+} neurons (Dopa (blue)) and no TH-td^{+} neurons (Normal (red)). (f) Overlap of signals from red (TH-td^{+}) and green (GCaMP6 or Fluo-4) fluorescence signal to generate a mask for cell identification. (g) Region of interest (ROIs) corresponding to individual neurons are identified and Identity numbers for each segmented neuron are assigned. (h) Firing traces and spike trains (red lines) are measured for each cell in (g). (i) Calcium transients are detected and their features (Inter Spike Interval (ISI), Amplitude (AMP), Increasing Rate (IR), Decreasing Rate (DR)) are estimated. (j) Statistical analysis is performed to estimate differences in calcium transient parameters between mutant (MUT) and gene corrected (WT) neuronal populations. (k) Further statistical analysis and classification are performed

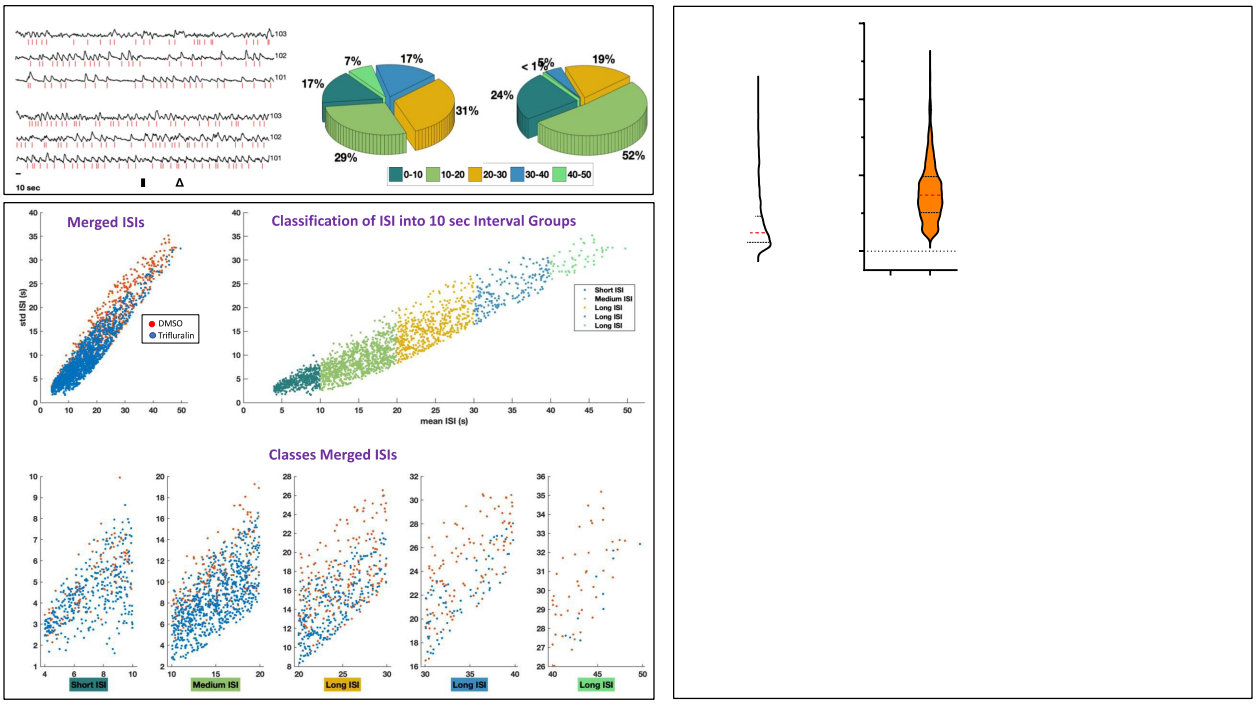

Figure 20. Effect of Trifluralin in GCaMP6-s calcium imaging assay on E46K-par1 differentiated neurons. The analysis was done using the Calcium image analysis pipeline. A) Representative traces for active neurons exposed to DMSO [0.2%] (i) and Trifluralin [2.5µM] (ii) after 3hr, pie chart showing the percentage distribution of active neurons according to Inter-Spike Interval (ISI) (iii). B) classification of mean ISIs for DMSO [0.2%] and Trifluralin [2.5µM] after 3hr exposure for merged ISIs (i), classification of ISIs into 10 sec interval groups (ii) and distribution of classes of merged ISIs (iii). C) Statistical analysis of calcium signal features for DMSO [0.2%] and Trifluralin [2.5µM] after 3hr exposure: Amplitude (i), ISI (ii), Removing rate (iii), Releasing rate (iv), Spike area (v), Spike width (vi), and Time to peak (vii).

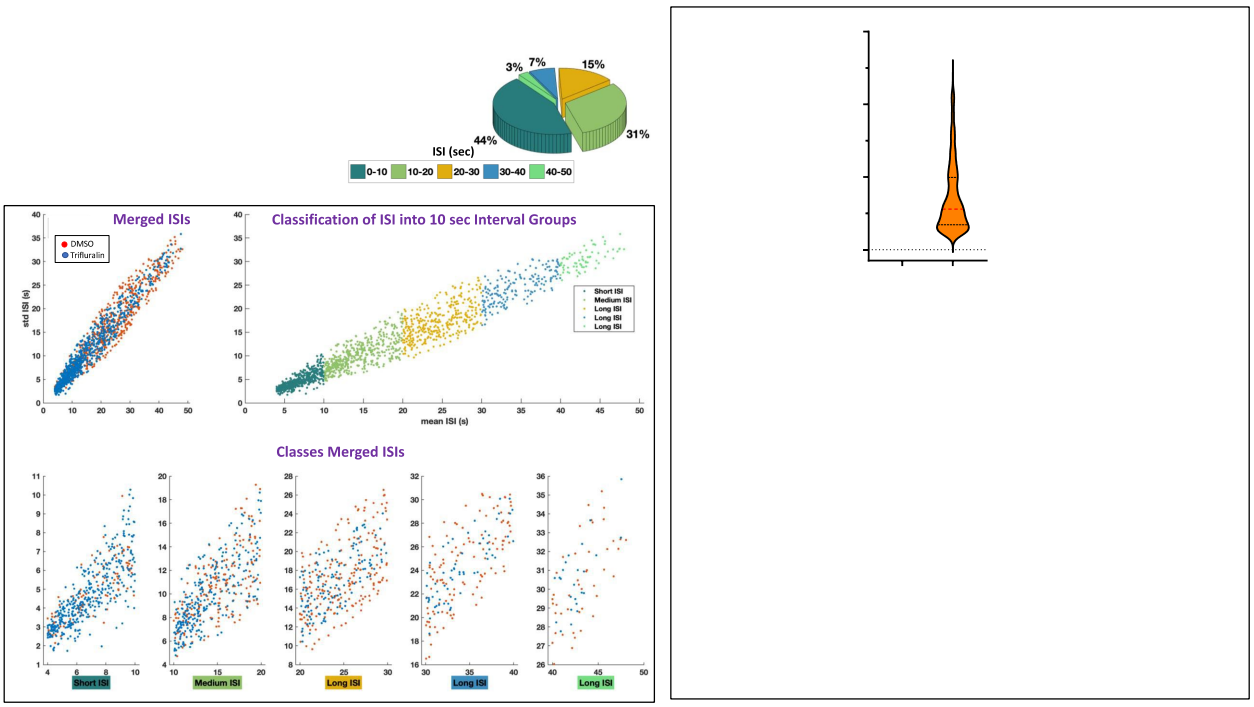

Figure 21. Effect of Trifluralin in GCaMP6-s calcium imaging assays on E46K-par1 differentiated neurons. The analysis was done using the Calcium image analysis pipeline. A) Representative traces for active neurons exposed to DMSO [0.2%] (i) and Trifluralin [2.5µM] (ii) after 24hr, pie chart showing the percentage distribution of active neurons according to Inter-Spike Interval (ISI) (iii). B) classification of mean ISIs for DMSO [0.2%] and Trifluralin [2.5µM] after 24hr exposure for merged ISIs (i), classification of ISIs into 10 sec interval groups (ii) and distribution of classes of merged ISIs (iii). C) Statistical analysis of calcium signal features for DMSO [0.2%] and Trifluralin [2.5µM] after 24hr exposure: Amplitude (i), ISI (ii), Removing rate (iii), Releasing rate (iv), Spike area (v), Spike width (vi), and Time to peak (vii).

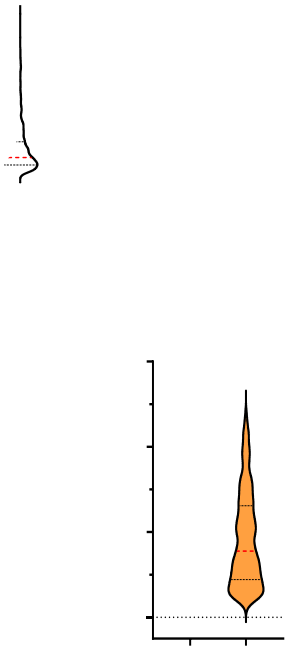

Figure 22. Statistical analysis of calcium signal features for E46K-par1 TH-td^{+} “Dopa” and non-TH-td^{+} “normal” differentiated neurons exposed to DMSO [0.2%] and Trifluralin [2.5µM]. A) After 3hr exposure: Amplitude (i), ISI (ii), Removing rate (iii), Releasing rate (iv), Spike area (v), Spike width (vi), and Time to peak (vii). B) After 24hr exposure: Amplitude (i), ISI (ii), Removing rate (iii), Releasing rate (iv), Spike area (v), Spike width (vi), and Time to peak (vii).

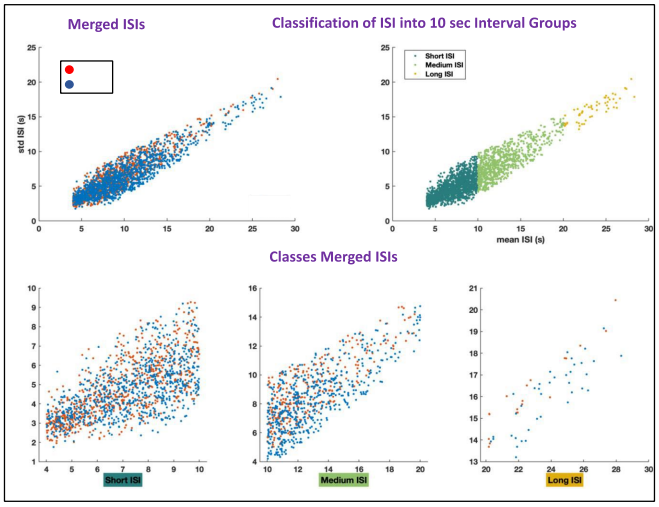

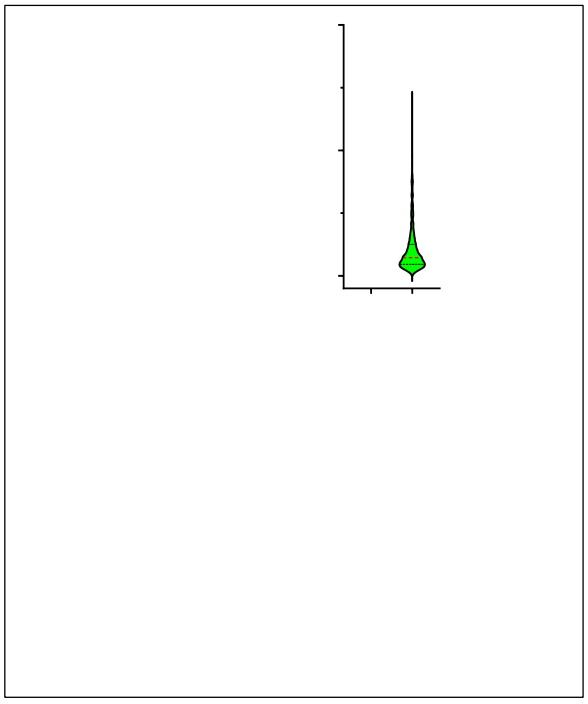

Figure 23. Effect of Copper Sulfate ($CuSO_4$) in GCaMP6-s calcium imaging assay on E46K-par1 differentiated neurons. The analysis was done using the Calcium image analysis pipeline. A) Representative traces for active neurons exposed to DMSO [0.2%] (i) and $CuSO_4$ [2.5µM] (ii) after 24hr, pie chart showing the percentage distribution of active neurons according to Inter-Spike Interval (ISI) (iii). B) classification of mean ISIs for DMSO [0.2%] and $CuSO_4$ [2.5µM] after 24hr exposure for merged ISIs (i), classification of ISIs into 10 sec interval groups (ii) and distribution of classes of merged ISIs (iii). C) Statistical analysis of calcium signal features for DMSO [0.2%] and $CuSO_4$ [2.5µM] after 24hr exposure: Amplitude (i), ISI (ii), Removing rate (iii), Releasing rate (iv), Spike area (v), Spike width (vi), and Time to peak (vii).

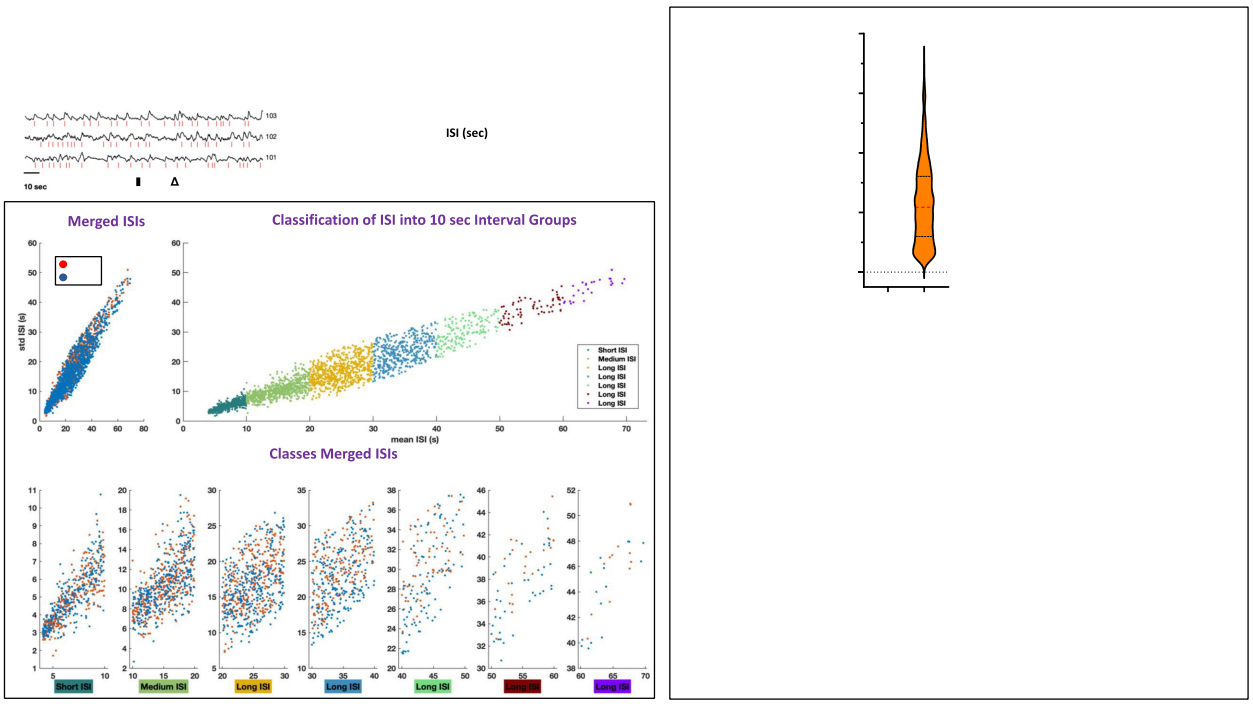

Figure 24. Effect of Copper Sulfate ($CuSO_4$) in GCaMP6-s calcium imaging assays on E46K-par1 differentiated neurons. The analysis was done using the Calcium image analysis pipeline. A) Representative traces for active neurons exposed to DMSO [0.2%] (i) and $CuSO_4$ [15µM] (ii) after 24hr, pie chart showing the percentage distribution of active neurons according to Inter-Spike Interval (ISI) (iii). B) classification of mean ISIs for DMSO [0.2%] and $CuSO_4$ [15µM] after 24hr exposure for merged ISIs (i), classification of ISIs into 10 sec interval groups (ii) and distribution of classes of merged ISIs (iii). C) Statistical analysis of calcium signal features for DMSO [0.2%] and $CuSO_4$ [15µM] after 24hr exposure: Amplitude (i), ISI (ii), Removing rate (iii), Releasing rate (iv), Spike area (v), Spike width (vi), and Time to peak (vii).

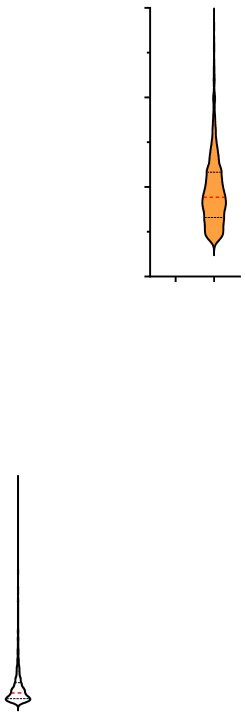

Figure 25. Statistical analysis of calcium signal features for E46K-par1 TH-td^{+} “Dopa” and non-TH-td^{+} “normal” differentiated neurons exposed to DMSO [0.2%] and $CuSO_4$ [2.5µM]. A) After 24hr exposure: Amplitude (i), ISI (ii), Removing rate (iii), Releasing rate (iv), Spike area (v), Spike width (vi), and Time to peak (vii). B) DMSO [0.2%] and $CuSO_4$ [15µM] after 24hr exposure: Amplitude (i), ISI (ii), Removing rate (iii), Releasing rate (iv), Spike area (v), Spike width (vi), and Time to peak (vii).

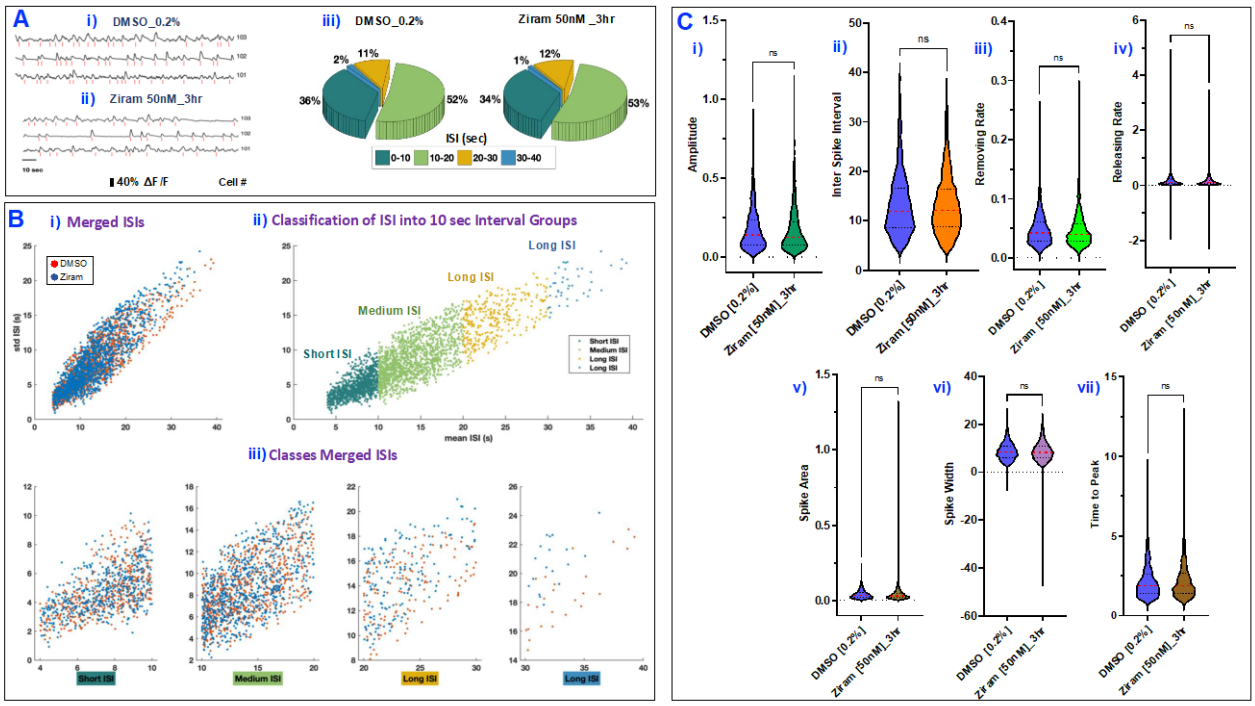

Figure 26. Effect of Ziram in GCaMP6-s calcium imaging assay on E46K-par1 differentiated neurons. The analysis was done using the Calcium image analysis pipeline. A) Representative traces for active neurons exposed to DMSO [0.2%] (i) and Ziram [50nM] (ii) after 3hr, pie chart showing the percentage distribution of active neurons according to Inter-Spike Interval (ISI) (iii). B) classification of mean ISIs for DMSO [0.2%] and Ziram [50nM] after 3hr exposure for merged ISIs (i), classification of ISIs into 10 sec interval groups (ii) and distribution of classes of merged ISIs (iii). C) Statistical analysis of calcium signal features for DMSO [0.2%] and Ziram [50nM] after 3hr exposure: Amplitude (i), ISI (ii), Removing rate (iii), Releasing rate (iv), Spike area (v), Spike width (vi), and Time to peak (vii).

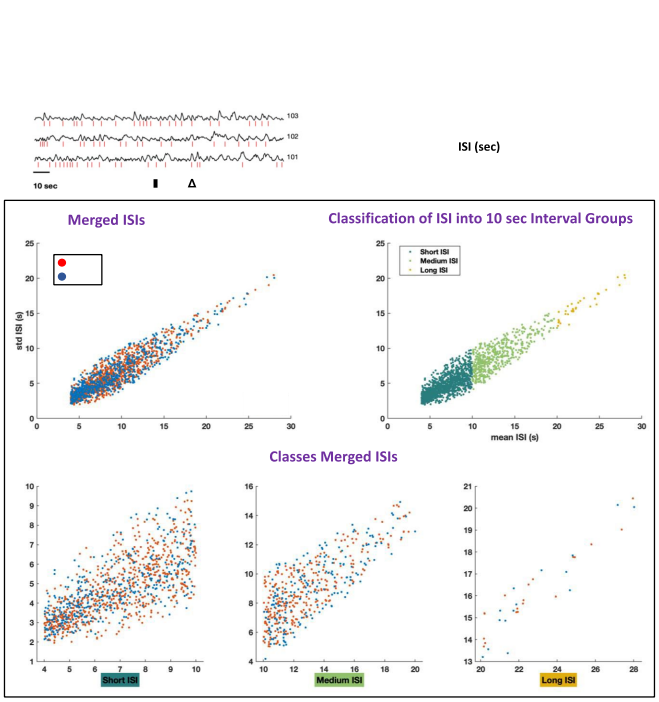

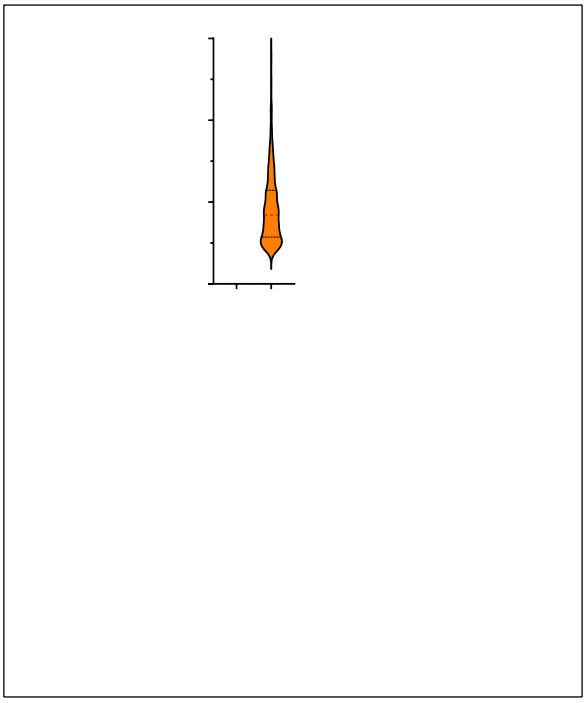

Figure 27. Effect of Ziram in GCaMP6-s calcium imaging assays on E46K-par1 differentiated neurons. The analysis was done using the Calcium image analysis pipeline. A) Representative traces for active neurons exposed to DMSO [0.2%] (i) and Ziram [50nM] (ii) after 24hr, pie chart showing the percentage distribution of active neurons according to Inter-Spike Interval (ISI) (iii). B) classification of mean ISIs for DMSO [0.2%] and Ziram [50nM] after 24hr exposure for merged ISIs (i), classification of ISIs into 10 sec interval groups (ii) and distribution of classes of merged ISIs (iii). C) Statistical analysis of calcium signal features for DMSO [0.2%] and Ziram [50nM] after 24hr exposure: Amplitude (i), ISI (ii), Removing rate (iii), Releasing rate (iv), Spike area (v), Spike width (vi), and Time to peak (vii).

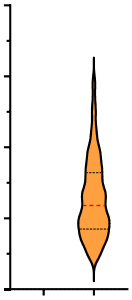

Figure 28. Statistical analysis of calcium signal features for E46K-par1 TH-td^{+} “Dopa” and non-TH-td^{+} “normal” differentiated neurons exposed to DMSO [0.2%] and Ziram [50nM]. A) After 3hr exposure: Amplitude (i), ISI (ii), Removing rate (iii), Releasing rate (iv), Spike area (v), Spike width (vi), and Time to peak (vii). B) DMSO [0.2%] and Ziram [50nM] after 24hr exposure: Amplitude (i), ISI (ii), Removing rate (iii), Releasing rate (iv), Spike area (v), Spike width (vi), and Time to peak (vii).

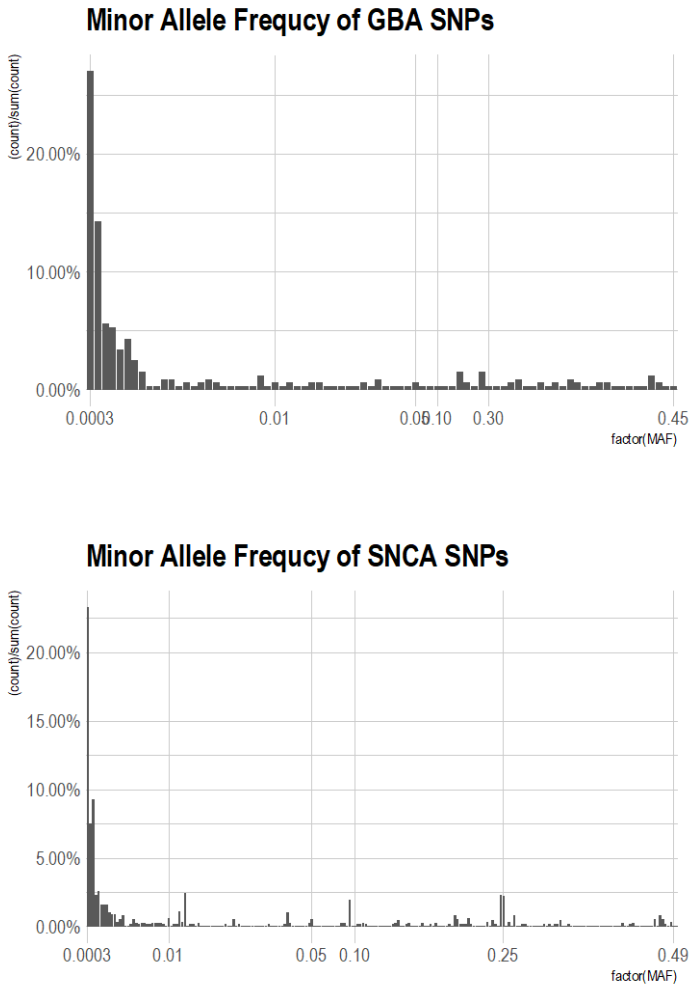

Figure 29 Minor allele frequency (MAF) for all variants with data in *GBA* and *SNCA*, in the PEG study (n=1870).

Figure 30: Results from the case-only GxE analysis in the PEG study, using a SNP-set kernel association test (SKAT) to test whether a higher burden of variants in the *SNCA* or *GBA* genes is associated with higher PD risk under pesticide exposure, using all PD-related pesticides. We show results for two different weighting schemes for handling rare variants, a weight designed to incorporate an assumption that rare variants are more likely to be causal variants with larger effect sizes, and a weight to incorporate more effects from common variants

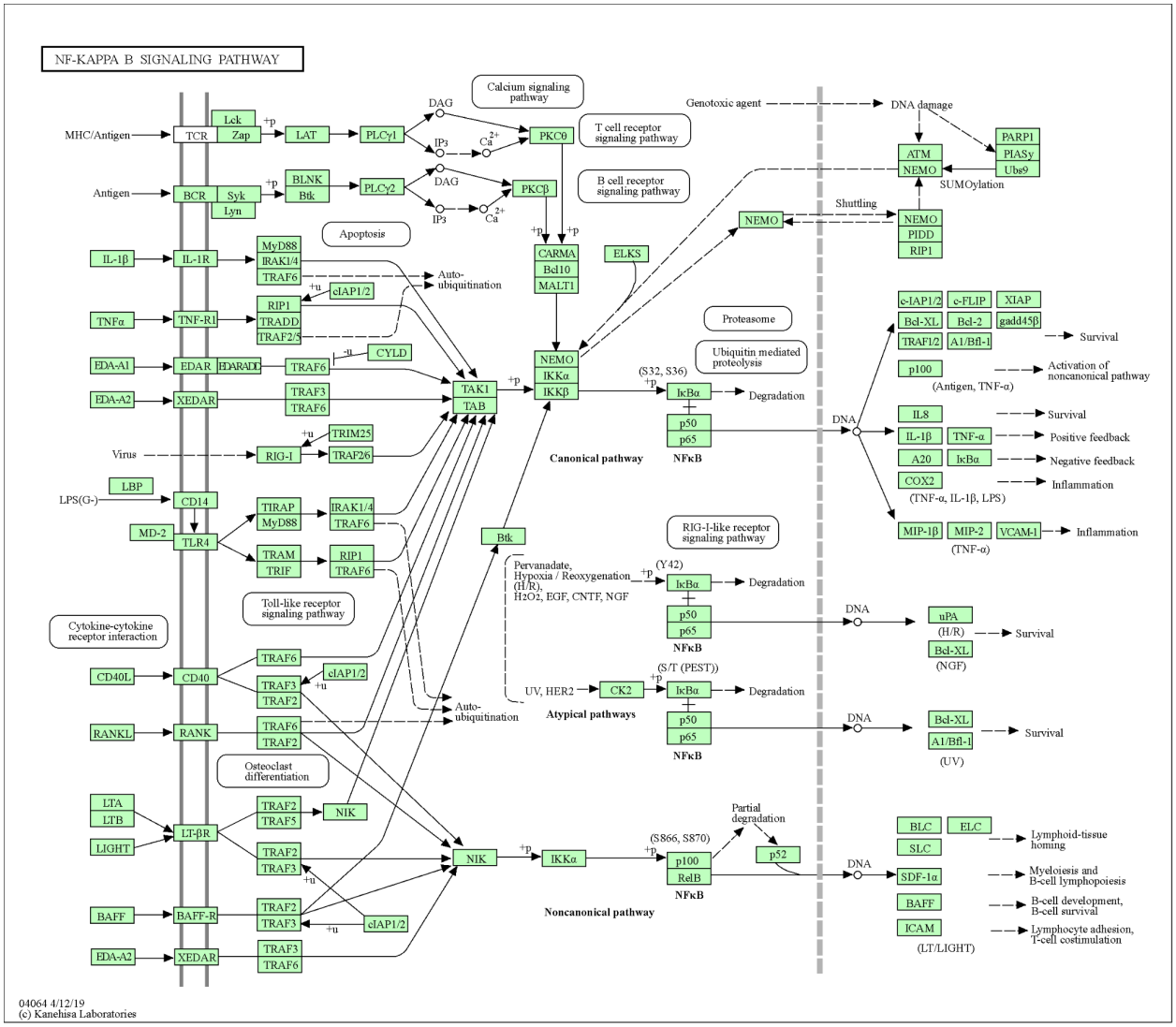

Figure 31. NF-κB pathway map. KEGG Pathway Database. https://www.genome.jp/pathway/hsa04064

What opportunities for training and professional development has the project provided?

Dr. Krolewski presented data from the project at the Parkinson's Study Group Annual Symposium and meeting. The meeting provided networking opportunities, included a poster presentation session as well. The theme of the symposium was "Parkinson's disease and the environment". Data from this project was also used as preliminary data for a successful K08 award application for Dr. Krolewski from NIEHS. This was awarded in November 2022. Dr. Ritz delivered the keynote address for the symposium.

How were the results disseminated to communities of interest?

Some results from this work are included in the manuscript that has been accepted in principle at Nature Communications and will be available to the broader scientific and lay community as a result. Additional work was published by the Ritz lab, see "Journal Articles" below.

What do you plan to do during the next reporting period to accomplish the goals?

Not applicable/nothing to report

4. **IMPACT:**

What was the impact on the development of the principal discipline(s) of the project?

The reagents developed by the Rubin lab (specifically the GBA reporter lines and the triplicated SNCA reporter line) will extend our ability to evaluate the effects of toxicants and compounds directly on dopaminergic neurons. These reagents will allow for clear evaluation of the sensitivity of dopaminergic neurons to various toxicants that people have been exposed to in the environment. Toxicants that cause cell death at lower doses will provide evidence to the field of gene/environment interactions and Parkinson's disease epidemiology. The findings will also prompt more in-depth mechanistic investigation of the implicated pesticides.

The results described by the Khurana lab provide the validation of gateway assays and conditions that can be used to characterize the effect of toxicants on differentiated dopaminergic neurons. This allows us to classify the toxicants according to their effect on the function of organelles (e.g. mitochondria), providing some clues into their mechanism of action beyond just information about the survival of cultured dopaminergic neurons. Trifluralin and Propargite are clear examples of a set of toxicants for which we quantified their effect on mitochondria at the biochemical level using the mitochondria subunit assay and at a functional level using the Agilent Seahorse XFCell Mito stress assay. Ideally, testing for metabolites in the culture conditions after exposure to toxicants would provide more information about the metabolic output of such effect on health and function of differentiated neurons, but at the moment we don't have the capabilities to generate these types of results.

In the PEG study, by analyzing all pesticides widely used in Central California, we implicate over 30 real-world pesticides most strongly associated with PD. This research provides epidemiologic evidence related to specific pesticides which can now be used to inform future lab-based experiments with novel pesticide targets and drive preventative policy around these patterns or agents. Furthermore, our work now integrating relevant genetics will inform further research in the lab, both as part of this project and beyond, related to genetic susceptibility related to pesticide exposures and PD.

What was the impact on other disciplines?

Nothing to report.

What was the impact on technology transfer?

Nothing to report

What was the impact on society beyond science and technology?

These data have potential to influence the recommendations regarding the widespread use of multiple agricultural or consumer products based on how likely they are to cause dopaminergic cell death. The work has potential to increase awareness concerning these products and safety protocols that should be put in place. The in vitro data showing death of dopaminergic neurons when exposed to certain toxicants combined with PEG pesticide exposure data indicating an association with PD strongly argues for additional studies on these toxicants and consideration of additional regulation of these pesticides and toxicants.

5. CHANGES/PROBLEMS:

Changes in approach and reasons for change

Due to budget and time constraints, attempts to recover a THtdtomato knock-in clone for the 2-copy isogenic line have been suspended. Limited analysis was performed on mixed cultures of the unmodified parental 2-copy clone using antibody staining for tyrosine hydroxylase and other neuronal markers to provide the necessary comparison data on toxicant sensitivity.

Actual or anticipated problems or delays and actions or plans to resolve them

Delays occurred as a result of the COVID-19 suspension of wet lab work. The delays we experienced put us a few months behind schedule on a limited set of tasks. We also encountered difficulties obtaining an ideal toxicant library. The Enzo toxicity library initially proposed has a high percentage of drugs with end organ toxicity. A library with primarily environmental or industrial toxicants would be a more ideal screening library. We have contacted NCATS to request access to a portion of their tox21 library, but have not yet been successful in obtaining a commitment to utilize the library. As described in previous technical reports, we compiled a small custom library from the list of PD-associated pesticides from the PEG data set described by our collaborators from the Ritz lab. The data from those experiments is presented above.

In the Khurana lab, we experienced a delay in the development and implementation of imaging and biochemical assays due to the COVID-19 suspension of non-essential laboratory activities. All of this notwithstanding, we have made substantial progress on assay development as noted above. However, thus far we are not yet at the point of being able to distinguish mutant from isogenic mutation-corrected controls with the assays we have developed.

Changes that had a significant impact on expenditures

Significant changes in use or care of human subjects, vertebrate animals, biohazards, and/or select agents

Nothing to report.

Significant changes in use or care of human subjects

Nothing to report.

Significant changes in use or care of vertebrate animals

Nothing to report.

Significant changes in use of biohazards and/or select agents

Nothing to report.

6. PRODUCTS:

- **Publications, conference papers, and presentations**

Dr. Krolewski presented work from this project as an invited platform presentation at the annual meeting of the Parkinson's Study Group in June 2022. The abstract was published in the Movement Disorders Journal: Movement Disorders, Vol. 37, Suppl. 1, 2022.

Dr. Khurana has been invited to present on determinants of variable penetrance of Parkinson's disease mutations by Spanish Neurology Society (Valencia November 2023) and, in part, he will be presenting this work.

Dr. Ritz is an invited speaker at the Society for Toxicology (SOT) meeting in Nashville in March 2023 and will present "OMICS studies of the Pesticides Exposome and Parkinson's disease in Rural Central California". Dr. Ritz also presented at the International Society for Environmental Epidemiology (ISEE) in Sept 2022 in Athens: "Geographic and Record-Based Pesticide Exposure Assessment, Biologic Exposure Signatures, and Chronic Disease Modelling in California". Dr. Ritz is invited to present at the World Parkinson's Congress (WPC) in Barcelona in July 2023 and will present: " Environmental Contributions to PD"

Journal publications.

A manuscript describing some of the work reported here, co-authored by Dr. Krolewski (Rubin lab), Dr. Lucumi Moreno (Khurana lab) and Dr. Paul (Ritz lab) with the three PIs (Ritz, Khurana, and Rubin) is recently accepted to Nature Communications (see manuscript in appendix) and will be published pending minor editorial and formatting changes. A pre-print version of the manuscript has been deposited onto the BioRxiv preprint server: https://doi.org/10.1101/2022.02.06.479305.

Additional published manuscript includes:
Paul KC, Ritz B. Epidemiology meets toxicogenomics: Mining toxicologic evidence in support of an untargeted analysis of pesticides exposure and Parkinson's disease. Environment International. Volume 170, December 2022, 107613

Books or other non-periodical, one-time publications.

Nothing to report

Other publications, conference papers and presentations. .

Nothing to report.

- **Website(s) or other Internet site(s)**

Nothing to report.

- **Technologies or techniques**

Nothing to report.

- **Inventions, patent applications, and/or licenses**

Nothing to report.

- **Other Products**

Nothing to report.

7. PARTICIPANTS & OTHER COLLABORATING ORGANIZATIONS

What individuals have worked on the project?

Effort is reported for final period of 04/01/2022-09/14/2022

Name: Lee Rubin, PhD
Project Role: PI
Researcher Identifier: 0000-0002-8658-841X
Nearest Person Month worked: 0.83
Contribution to Project: Experiment planning, data analysis, coordination with co-PIs, supervision of Rich Krolewski, Gizem Rizki, Jack Blank

Name: Richard Krolewski, MD, PhD
Project Role: Scientist
Research Identifier: N/A
Nearest person month worked: 1.65
Contribution to project: Experiment planning, data analysis, coordination/project management, generation of transgenic lines, dopaminergic neuron experiments, supervision of Jack Blank.
*Dual appointment-Paid through a professional services billing agreement with Brigham and Women's Hospital

Name: Vikram Khurana, MD, PhD
Project Role: PI
Nearest Person Month worked: 1
Contribution to Project: Analysis planning, results interpretation, coordination with co-PIs, supervision of Edinson Lucumi

Name: Edinson Lucumi, PhD
Project Role: Postdoctoral Scholar
Nearest Person Month worked: 6
Contribution to Project: Image analysis, biochemical assay development, dopamine neuron experiments, data analysis

Name: Beate Ritz, MD, PhD
Project Role: PI
Nearest Person Month worked: 1.5
Contribution to Project: Analysis planning, results interpretation, coordination with co-PIs, supervision of Kimberly Paul

Name: Kimberly Paul, PhD
Project Role: Postdoctoral Scholar (until Dec 31, 2020)/Asst Prof of Neurology (Jan 1, 2021-current)
Nearest Person Month worked: 1
Contribution to Project: All epidemiologic analysis, including analysis planning, data analysis, results presentation, and interpretation

Has there been a change in the active other support of the PD/PI(s) or senior/key personnel since the last reporting period?

N/A final report

What other organizations were involved as partners?

Due to the nature of this partnering PI award, individuals working on the project from each of the three institutions (Rubin lab- Harvard/FAS; Khurana lab-BWH/Harvard; Ritz lab- UCLA) via video conference meetings and exchange of data. Other than this partnership, there is nothing to report from the Rubin, Khurana and Ritz labs.

8. SPECIAL REPORTING REQUIREMENTS

COLLABORATIVE AWARDS:

QUAD CHARTS:

9. APPENDICES:

- "Paul Krolewski Merged Manuscript resubmit.pdf"
- "Harvard Equipment Listing"